Q. J. R. Meteorol. Soc. (1994), **120**, pp. 881–922 551.513.1:551.515.41:551.515.51(213)

Mean climate and transience in the tropics of the UGAMP GCM: Sensitivity to convective parametrization

By JULIA SLINGO[1]*, MIKE BLACKBURN[1], ALAN BETTS[2], ROGER BRUGGE[1], KEVIN HODGES[1], BRIAN HOSKINS[1], MARTIN MILLER[3], LOIS STEENMAN-CLARK[1] and JOHN THUBURN[1]

[1]*University of Reading, UK*, [2]*Pittsford, USA and* [3]*European Centre for Medium-range Weather Forecasts, UK*

(Received 4 June 1993; revised 18 November 1993)

SUMMARY

The sensitivity of the UK Universities Global Atmospheric Modelling Programme (UGAMP) General Circulation Model (UGCM) to two very different approaches to convective parametrization is described. Comparison is made between a Kuo scheme, which is constrained by large-scale moisture convergence, and a convective-adjustment scheme, which relaxes to observed thermodynamic states. Results from 360-day integrations with perpetual January conditions are used to describe the model's tropical time-mean climate and its variability. Both convection schemes give reasonable simulations of the time-mean climate, but the representation of the main modes of tropical variability is markedly different. The Kuo scheme has much weaker variance, confined to synoptic frequencies near 4 days, and a poor simulation of intraseasonal variability. In contrast, the convective-adjustment scheme has much more transient activity at all time-scales. The various aspects of the two schemes which might explain this difference are discussed. The particular closure on moisture convergence used in this version of the Kuo scheme is identified as being inappropriate.

1. INTRODUCTION

This paper describes the ability of the UK Universities Global Atmospheric Modelling Programme (UGAMP) General Circulation Model (hereafter referred to as the UGCM) to simulate the time-mean climate and the transience of the tropics, with particular reference to their sensitivity to convective parametrization. Since the climate of a region is constructed from the ensemble of the weather systems that affect that region, it is important that general circulation models (GCMs) should be capable of representing the range of interacting space- and time-scales that make up that climatic mean. Thus, whilst the physical parametrizations in a GCM are developed and modified so as to ensure that the errors in representing today's climate means are minimized, they should also be validated in terms of their transient characteristics.

The release of latent heat by cumulus convection is the primary process by which the solar energy input to the equatorial regions is transferred to the upper troposphere and thence polewards by the Hadley circulation. In a time-mean sense, the Hadley circulation in January is dominated by the three major heat sources associated with Indonesia, South America and South Africa. In turn, the time-averaged tropical circulation is basically driven by the time-mean distribution of the diabatic heating (e.g. Webster 1983). Errors in the simulated tropical circulation can often be related to errors in the mean distribution of the heating (e.g. Miller *et al.* 1992), consistent with the results of idealized studies (e.g. Sardeshmukh and Hoskins 1988).

It is clear from satellite observations that the seasonal mean distribution of diabatic heating is built up from a variety of space- and time-scales (e.g. Lau *et al.* 1991). These range from the individual clouds, to the cloud clusters associated with synoptic-scale disturbances, to the super clusters or ensembles of clusters. These super clusters often display eastward propagation, characteristic of the intraseasonal oscillation as first described by Madden and Julian (1972). Periodicities in convective activity can often be identified; a period of 4 days over north Africa and the Atlantic associated with African easterly waves (Reed *et al.* 1977), 4 to 5 days over the west Pacific (Liebmann and

* Corresponding author: Centre for Global Atmospheric Modelling, UK Universities Global Atmospheric Modelling Programme, Department of Meteorology, University of Reading, Reading RG6 2AU, UK.

Hendon 1990), and 6 to 7 days over the east Pacific (Tai and Ogura 1987). These periodicities appear to be related to dynamical structures that have a coherent vertical structure and horizontal scale related to equatorial waves, such as Rossby-gravity waves (e.g. Hendon and Liebmann 1991).

This organization of tropical convection is important for a variety of reasons. The development and maintenance of equatorial waves is crucial for forecasting in the tropics. Tropical weather systems may also influence the extratropics by their direct migration polewards into the mid-latitude storm tracks. The diabatic heating over the region of high sea surface temperatures (SSTs) in Indonesia and the west Pacific (known as the warm pool) often displays intraseasonal variations. Variations at these lower frequencies may induce a far-field response in the extratropics with a suggestion that lack of activity at these time-scales in the tropics may be linked to a reduced incidence of blocking events in the extratropics (Ferranti *et al.* 1990). It is also believed that the spectrum of wave activity emanating from the tropical troposphere may be instrumental in the excitation of the stratospheric quasi-biennial oscillation and semi-annual oscillation (see, for example, Andrews *et al.* (1987) and references therein).

Despite the substantial evidence that organized tropical convection has a fundamental role in the general circulation, its detailed simulation by GCMs has received relatively little attention. A paper by Slingo *et al.* (1992) demonstrated that a high-resolution GCM may have considerable skill in representing the various spatial and temporal scales of tropical convection. In this paper, integrations of the UGCM at lower horizontal resolution are used to assess the sensitivity of the time-mean tropical circulation and the transient component of tropical heating to the parametrization of moist convective processes. The results from two 360-day perpetual January integrations are compared. The first integration used a version of the Kuo scheme (Tiedtke *et al.* 1988) as given in the original formulation of the UGCM; the second integration used the convective-adjustment scheme of Betts and Miller (1993).

Section 2 provides a basic description of the UGCM, section 3 outlines the two convection schemes used in this study, while the details of the integrations are given in section 4. The time-mean climate from each integration is described in section 5, and section 6 focuses on the characteristics of the tropical transience from each convection scheme. Finally, a discussion of the implications of these results and the reasons for the diverse behaviour of the model with differing convection schemes are given in section 7.

2. Model description

The UGCM is based on cycle 27 of the European Centre for Medium-range Weather Forecasts (ECMWF) model, which was operational in the summer of 1987. The model has 19 levels in the vertical, represented by a hybrid sigma/pressure coordinate (Simmons and Burridge 1981; Table 1). In the horizontal the prognostic variables are represented by a truncated series of spherical harmonics (Simmons *et al.* 1989). In the integrations described in this paper a horizontal resolution of T42 is used, that is isotropic or 'triangular' truncation at total wave number 42. Contributions to tendencies from parametrization schemes are calculated on a Gaussian grid of 128 (longitude) and 64 (latitude) points, where the mesh size is approximately 2.8°.

Basic descriptions of the dynamical aspects and physical parametrizations of the model can be found in Simmons *et al.* (1989) and Tiedtke *et al.* (1988) respectively. Subsequently various changes have been made to the model, some of which stem from improvements in the physical processes developed at the ECMWF; these changes are

described below. Table 2 summarizes the basic features of the UGCM as used in this paper.

(*a*) *Radiation*

In May 1989 the ECMWF made a major revision to its operational model, including substantial changes to the parametrization schemes. The radiation parametrization was

TABLE 1. VERTICAL COORDINATES USED IN THE UGCM

Model level	$A_{k+1/2}$	$B_{k+1/2}$	$\eta_{k+1/2}$	η_k
0	0	0	0	—
1	2000	0	0.0197	0.0099
2	4000	0	0.0395	0.0296
3	6046	0.0003	0.0600	0.0497
4	8268	0.0034	0.0850	0.0725
5	10610	0.0131	0.1178	0.1014
6	12851	0.0341	0.1609	0.1393
7	14698	0.0706	0.2157	0.1883
8	15861	0.1259	0.2825	0.2491
9	16116	0.2012	0.3603	0.3214
10	15357	0.2955	0.4471	0.4037
11	13621	0.4054	0.5398	0.4935
12	11102	0.5249	0.6345	0.5872
13	8127	0.6461	0.7263	0.6804
14	5125	0.7597	0.8103	0.7683
15	2550	0.8564	0.8816	0.8459
16	783	0.9287	0.9365	0.9090
17	0	0.9730	0.9730	0.9547
18	0	0.9923	0.9929	0.9826
19	0	1.0000	1.0000	0.9961

$\eta_{k+1/2} = A_{k+1/2}/P_{\text{ref}} + B_{k+1/2}$ where k is the model level and $P_{\text{ref}} = 1013.25$ hPa

TABLE 2. BASIC DESCRIPTION OF THE UGCM AS USED IN THIS PAPER

Domain	Global
Dependent variables	ζ, D, T, q, $\ln(p_s)$
Vertical coordinate	Hybrid, 19 levels
Vertical discretization	Simmons and Burridge (1981); vertical advection by flux-limited scheme (Thuburn 1993)
Horizontal discretization	Spectral, triangular truncation at T42
Horizontal grid	Gaussian, 128 longitude × 64 latitude
Time integration	Leap-frog for dynamics, forward for physical parametrization, semi-implicit ($\Delta t = 30$ min)
Time filter	Asselin (1972), $\epsilon = 0.1$
Lateral dissipation	Linear, ∇^6, $\tau = 4$ hours at $n = 42$, $K = 7.88 \times 10^{26}$ m^6 s^{-1}
Orography	Envelope, enhanced by one standard deviation
Gravity-wave drag	As Palmer *et al.* 1986
Vertical diffusion	Stability dependent, up to $\eta = 0.65$
Surface turbulent fluxes	Dependent on local roughness length and stability Minimum near-surface wind (3 m s^{-1}) imposed Convective gustiness included
Precipitating convection	Kuo (Tiedtke *et al.* 1988)
Shallow convection	Enhanced vertical diffusion of θ, q only (Tiedtke *et al.* 1988)
Large-scale condensation	Grid-scale saturation, evaporation of precipitation
Radiation	Interactive clouds, diurnal cycle, surface albedo modified by snow cover (Morcrette 1990)
Clouds	Empirical fractional cloudiness (Slingo 1987)
Land surface temperatures	Three-layer soil model, prescribed seasonal deep-soil temperature
Land soil moisture	Three-layer soil model, 20 cm capacity, prescribed seasonal deep-soil moisture
Sea surface temperatures	Fixed

replaced by the scheme developed and described by Morcrette (1990). Reasons for changing the radiation code included a stratospheric warm-temperature bias, a poor simulation of the outgoing long-wave radiation, and insufficient clear-sky atmospheric cooling with hence a too weak hydrological cycle (Arpe 1988). Morcrette (1990) showed that changing the radiation scheme, alone, could improve many aspects of the model's climate, particularly the Hadley circulation and the energetics of the mid-latitude baroclinic systems. For these reasons it was considered desirable to replace the existing UGCM radiation code by Morcrette's. Overall, the impact of the new code on the performance of the UGCM was very similar to that reported by Morcrette (1990) after its implementation in the ECMWF model, and so the results will only be summarized here. A more vigorous hydrological model and, consequently, a better Hadley circulation were simulated. The model was more dynamically active with increases in both the available potential energy and the eddy kinetic energy. The simulation of the southern hemisphere depression belt and the level of transient kinetic energy were markedly improved.

(*b*) *Surface fluxes*

A major shortcoming of the original version of the UGCM, as used in Boer *et al.* (1991), was a shift polewards of the subtropical jets, and excessive upper tropospheric easterlies in the tropics. The model failed to simulate the upper tropospheric equatorial westerlies in the central and east Pacific in January, which had implications for Rossby-wave propagation into, and from, the extratropics. Recently, the ECMWF has had some success in removing tropical upper tropospheric easterly errors by increasing the precipitation and partially eliminating the double Inter-Tropical Convergence Zone (ITCZ) structure over the warm pool of Indonesia and the west Pacific (Miller *et al.* 1992). This was achieved by enhancing the surface evaporation in regions of low surface wind speed, characteristic of the warm pool, through a reformulation of the transfer coefficients. However, Miller *et al.* emphasized that at that time there was very little experimental data to support this change, so a more pragmatic approach has been used in the UGCM. A minimum near-surface wind speed (v_m) has been imposed in the calculation of the surface turbulent fluxes. This is intended to represent the variability of the near-surface winds associated with subgrid-scale turbulence. Such an approach has been used in a model of the upper equatorial Pacific Ocean (Gent 1991) to allow for the underestimation of the mean wind speed when using the speed of the mean wind. In addition, an attempt to allow for the subgrid-scale gustiness (v_c) associated with deep convection has also been included. In the integrations described in this paper, the near-surface wind, u_1, is given by,

$$u_1 = \{(\max(|u_g|, v_m))^2 + v_c^2\}^{1/2} \tag{1}$$

for grid points with precipitating convection, otherwise:

$$u_1 = \max(|u_g|, v_m) \tag{2}$$

u_g is the grid-point wind at the lowest model level and v_m and v_c are constant speeds, both assumed to be $3\ \mathrm{m\ s^{-1}}$. Since these integrations were completed, the preliminary results of TOGA COARE* have supported the approach used by Miller *et al.* (1992) and a review of the surface flux parametrization in the UGCM is planned.

As with the ECMWF model (Miller *et al.* 1992), several aspects of the simulated time-mean climate in the UGCM were dramatically improved when the enhanced surface

* Tropical Ocean and Global Atmosphere programme Coupled Ocean–Atmosphere Response Experiment.

fluxes were implemented with the Kuo convection scheme. These improvements will be described briefly here. In response to the modification to the near-surface wind formulation, the latent-heat flux increased over much of the tropics, but especially in the west Pacific. There were substantial changes in the distribution of convective rainfall, with an increase in precipitation over the warm pool and partial elimination of the split ITCZ. This led to marked improvements in both the divergent and rotational components of the time-mean tropical circulation. The excessive upper tropospheric easterlies were dramatically reduced and the transition region between easterlies and westerlies moved equatorwards in both hemispheres.

In January the simulation of the upper tropospheric westerlies in the central and east Pacific was improved, an important result since this region, the Pacific wave guide, is where interactions with the extratropics are known to occur (e.g. Kiladis and Weickmann 1992). It is interesting to note that, even though the Walker circulation was enhanced by the additional heating over the warm pool, the implied increase in the westerly divergent wind was only about $1\ \mathrm{m\,s^{-1}}$. Thus most of the change in the zonal wind gradient across the Pacific was associated with the rotational flow. The asymmetric upper tropospheric stream-function anomaly, produced with the enhanced surface fluxes, showed the development of a forced stationary Rossby mode, with a cyclonic dipole downstream of the main area of increased heating in the west Pacific. Such a result was consistent with that predicted by Sardeshmukh and Hoskins (1988) from the nonlinear response of a barotropic flow to imposed steady-state divergence (their Fig. 16).

In summary, the radiation change had a global influence on the heating distribution, and a profound effect on the circulation and energetics of the model, particularly the extratropical transient eddies. On the other hand the surface flux change had a more local and direct effect on the tropical circulation, reducing the easterly zonal wind error and improving the simulation of the Pacific Walker circulation. The main improvements associated with both these changes can be summarized as follows:

(i) Intensification of the hydrological cycle.
(ii) Strengthening of the Hadley and Ferrel cells.
(iii) Reduction in the model's temperature errors, particularly in the tropical troposphere and in the stratosphere.
(iv) Reduction in the tropical easterly error and improvements in the upper branch of the Walker circulation.
(v) Substantial increase in the transient eddy kinetic energy in the southern hemisphere depression belt.
(vi) Better simulation of the earth's radiation budget.

(c) *Vertical advection and diffusion*

The UGCM incorporates two changes to the treatment of vertical differencing used in cycle 27 of the ECMWF model. The original centred-difference scheme for vertical advection has been replaced by the flux-limited scheme described by Thuburn (1993); the parametrization of vertical diffusion has been switched off above $\eta = 0.650$ (where η = pressure/surface pressure) in both statically stable and unstable situations. This latter change is similar to that introduced at the ECMWF in January 1988, whose effects are described by Miller (1988) and Palmer *et al.* (1990).

The original vertical-advection scheme was based on quasi-second-order centred differences. This scheme has a tendency to generate oscillations in the profile of an advected quantity where its gradient changes rapidly. In particular, it leads to negative moisture values above the subtropical inversion, and to noisy temperature profiles near

the tropopause. To avoid these problems a simple flux-limited scheme was used for vertical advection in these simulations. In this scheme judicious combinations of centred and upwind differences are chosen at the horizontal faces of each grid box to ensure that no spurious oscillations are produced. A full description of the implementation of this scheme in the UGCM can be found in Thuburn (1993).

Palmer *et al.* (1990) reported a possible sensitivity of the simulated blocking frequency in the northern hemisphere winter storm tracks to the removal of vertical diffusion above the planetary boundary layer. In extended 30-day forecasts they found a higher simulated blocking frequency in 1987/88, following the change in the operational model. However, their results do not distinguish between changes in model formulation and interannual variability in blocking frequency. A more unequivocal effect of the vertical-diffusion change, seen by both Miller (1988) and Palmer *et al.* (1990), was a correction of the continued loss of eddy kinetic energy in the extratropics throughout the forecast period.

Experimentation with vertical diffusion in the UGCM has shown increased kinetic energy in the subtropics associated with upper-level troughs propagating equatorwards at the ends of the storm tracks, and strengthened westerly flow over the equatorial east Pacific and Atlantic Oceans. The low-order flux-limited scheme used here is certain to partially offset the effects of removal of vertical diffusion in the free atmosphere, since it is somewhat diffusive in the presence of strong vertical gradients, compared with the second order centred-difference scheme (see Thuburn 1993). There do not appear to be numerical problems associated with static instability when vertical diffusion is suppressed with the flux-limited advection scheme.

3. Convective parametrization

The original version of the UGCM used the Kuo (1974) deep-convection scheme, in conjunction with a diffusive shallow-convection scheme, as implemented in the ECMWF model (Tiedtke *et al.* 1988). As part of an extensive programme of research within UGAMP to study the representation of convective processes it was decided to assess the sensitivity of the UGCM to another parametrization. The convective-adjustment scheme of Betts (1986) and Betts and Miller (1993) was deemed a suitable alternative because it uses a substantially different approach to the representation of convective processes. In particular, it does not require an estimate of the moisture convergence to close the set of predictive equations, and the parametrization of shallow convection was considered to be more physically reasonable.

(*a*) *Kuo scheme*

The parametrization of deep, precipitating convection is based on the principles of Kuo (1974), in which the heating and moistening by cumulus clouds are related to the local moisture supply from large-scale convergence of moisture and surface evaporation. Variants of this scheme are widely used in GCMs (e.g. Gates 1992).

As formulated in the UGCM, convection is initiated by lifting near-surface air to the condensation level, defined as cloud base (p_b). The cloud-temperature (T_c) and humidity (q_c) profiles are then computed assuming moist adiabatic ascent from the cloud base, including modification by the effects of condensation. Two iterations are used in the condensation calculation. Cloud top (p_t) is defined as the level of non-buoyancy. Even if adiabatic ascent identifies a cloud layer, precipitating convection is only permitted if there is large-scale accession of moisture ($Q_{ac} > 0$) when integrated from the surface to the top of the cloud layer:

$$Q_{ac} = E - \frac{1}{g}\int_{p_s}^{p_t} \nabla . (q\mathbf{V})\, dp \tag{3}$$

where g is gravity and $q\mathbf{V}$ the humidity vector wind. As in Kuo (1965), Eq. (3) includes the effects of surface evaporation (E) as well as the atmospheric convergence of moisture. If the condition $Q_{ac} > 0$ is not satisfied then the shallow-convection scheme (described below) is used.

Once the cloud profiles are known, the vertical distributions of moistening (Δq) and heating (ΔT), and hence precipitation production by deep convection, can be determined. These are controlled by the moisture accession (Q_{ac}) and the parameter, β, which determines the partitioning of the moisture supply between heating and moistening of the environment. Following Anthes (1977), we use

$$\beta = \left(\frac{(1 - \overline{RH}}{(1 - RH_{crit})}\right)^n \qquad \text{for } \overline{RH} \geqslant RH_{crit} \tag{4}$$

otherwise $\beta = 1$. $\overline{RH}$ is the mean relative humidity of the cloud layer, and RH_{crit} is a critical relative humidity below which only moistening of the environment occurs. The most appropriate form of β to use is uncertain and the performance of the model is sensitive to its formulation (Tiedtke *et al.* 1988). Following Tiedtke *et al.* (1988), the UGCM uses a cubic form ($n = 3$) and a value of zero for RH_{crit}. This means that whenever there is a deep convection, there is always some heating (i.e. precipitation formation) regardless of the dryness of the environment.

The moistening and heating profiles are given by:

$$\Delta q = \frac{\beta Q_{ac}(q_s(T_e) - q_e)}{\int_{p_b}^{p_t} (q_s(T_e) - q_e) dp} \tag{5}$$

$$\Delta T = \frac{(1 - \beta) Q_{ac}(T_c - T_e)}{\int_{p_b}^{p_t} (T_c - T_e) dp} \tag{6}$$

where T_e and q_e are the temperature and humidity of the environment and q_s is the saturated humidity mixing ratio. q_c is assumed to be equal to saturation at T_e.

The total release of convective precipitation is determined directly from the heating profile, but the net convective precipitation reaching the surface is modified by the evaporation of falling rain into the environment below cloud base. Thus, in the Kuo scheme, both the incidence of deep convection and the amount of precipitation released are controlled by the large-scale accession of moisture.

As already stated, if a cloud layer is identified but there is no large-scale moisture accession, then the Kuo scheme does not operate. In these circumstances it is assumed that shallow non-precipitating cumulus clouds are present. The Kuo scheme is not designed to represent the effects of such clouds; instead a specific parametrization of shallow convection is used as described in Tiedtke *et al.* (1988). This assumes that the effects of shallow cumulus convection on the large-scale flow can be described by the turbulent fluxes of dry static energy ($\bar{s}$) and moisture ($\bar{q}$), where the overbar denotes the grid-scale average. These fluxes are parametrized using an eddy diffusivity approach:

$$\frac{\partial \bar{s}}{\partial t} = \frac{1}{\bar{\rho}} \frac{\partial}{\partial z}\left(\bar{\rho} K \frac{\partial \bar{s}}{\partial z}\right) \tag{7}$$

$$\frac{\partial \bar{q}}{\partial t} = \frac{1}{\bar{\rho}} \frac{\partial}{\partial z} \left(\bar{\rho} K \frac{\partial \bar{q}}{\partial z} \right) \tag{8}$$

where $\bar{\rho}$ is the grid-scale average density and z is height. Equations (7) and (8) are applied within the cloud layer (as defined by the Kuo scheme, but with an upper limit on the cloud-top height of 1600 m) and in the inversion layer above cloud top. The eddy diffusion coefficient, K, is assumed to be constant throughout the cloud layer, but is dependent on the strength of the humidity gradient within the inversion layer:

$$K = \begin{cases} K_0 & \text{Active cloud layer} \\ K_0 \dfrac{(RH - 0.8)}{0.2} \Delta RH & \text{Inversion} \\ 0 & \text{Elsewhere.} \end{cases} \tag{9}$$

As in Tiedtke *et al.* (1988), $K_0 = 10\ \mathrm{m^2\ s^{-1}}$. RH is the relative humidity below the inversion and ΔRH is the change in relative humidity across the inversion.

(*b*) *The convective-adjustment scheme*

The convective-adjustment scheme, as formulated by Betts (1986), is designed to represent, directly, the quasi-equilibrium thermodynamic state of the atmosphere that is established by shallow and deep convection in response to radiative and dynamical forcing. The scheme is essentially a lagged adjustment towards calculated reference profiles, where the profiles are based on the observed thermodynamic structure of the atmosphere in convective situations. The version of the scheme implemented in the UGCM was developed at the ECMWF, and is essentially as described in Betts and Miller (1993). Hereafter it will be referred to as BM93 to distinguish it from other versions of the scheme used in the literature.

The scheme treats deep and shallow convection as separate processes that can only operate singly at any grid column. The designation of a column as shallow or deep is achieved by determining the cloud base and cloud top using a simple lifting process, as in the Kuo scheme. In the UGCM, shallow convection is initiated if the cloud top is below the level of $\sigma = 0.725$ over land, or $\sigma = 0.810$ over sea, where σ = pressure/surface pressure. This differentiation between land and sea is a simple parametrization to allow for the tendency for shallower clouds to precipitate over the oceans. In addition, if the deep convection is found to be non-precipitating because the environment is too dry then the column is designated shallow and the cloud top is set to the prescribed upper limit of $\sigma = 0.725$. If air from the near-surface layer is not buoyant, parcel ascents are attempted from all levels up to the mid-troposphere, to allow for the possibility of mid-level convection. Multiple convecting layers within a column are not allowed.

It has been noted from observations (see Betts (1986)) that, in the presence of extensive deep convection, the atmospheric thermal structure remains slightly unstable with respect to the wet virtual adiabat (which includes the effect of liquid water loading), at least up to the freezing level. Above the freezing level a more stable structure is observed, associated with both the freezing process and the fallout of precipitation which reduces the ice and water loading. Thus the temperature reference profile for deep convection is determined by assuming a lapse rate which is slightly unstable with respect to the wet virtual adiabat below the freezing level. Above the freezing level the reference profile returns, at cloud top, to the moist adiabat from the cloud base. The base temperature for the reference profile for deep convection is determined from the average of the environment and cloud temperatures at the top of the sub-cloud layer, defined as $\eta = 0.909$ in the UGCM. Here, the cloud temperature corresponds to that determined

by the simple lifting of near-surface air, described above. The humidity reference profile for deep convection is computed from the temperature reference profile by specifying the subsaturation pressure deficit ($\mathcal{P} = p^* - p$, where p^* is saturation pressure) at three levels (cloud base (−25 hPa), freezing (−40 hPa) and cloud top (−20 hPa)) and linearly interpolating $\mathcal{P}$ between them. Thus, along with the relaxation time, the specification of the subsaturation essentially controls the relative humidity of the environment.

The interaction of deep convection with the boundary layer is crucial, especially over the oceans where the surface temperature is fixed. The scheme includes a simple parametrization of the low-level cooling and drying by convective downdraughts. For the three model levels (defined as the subcloud layer) a different reference profile is used, related to a simple unsaturated downdraught which originates at a single level near 850 hPa and descends at constant equivalent potential temperature, θ_e, and constant subsaturation. An adjustment time-scale for the boundary layer is determined from the downdraught evaporation efficiency, i.e. the ratio of the rate of evaporation into the downdraught to the precipitation rate. This must be prescribed, and the UCGM currently uses a value of 0.15. A fuller description of the downdraught parametrization can be found in Betts and Miller (1993).

In order to conserve energy within the parametrization of deep convection the constraint is applied that the difference between the total moist enthalpy ($C_pT + Lq$, where C_p is the specific heat at constant pressure and L the latent heat) of the environment and the reference profile must integrate to zero through the convective layer. To achieve this the reference temperature is corrected at each level in two iterations. The precipitation rate is then calculated from the difference between the moisture content of the reference and environment profiles, integrated over the convecting layer (see Betts and Miller (1993)). If the precipitation rate is negative, shallow convection is invoked instead.

Shallow convection is parametrized as a mixing process involving air below cloud base and air at, and above, the capping inversion top. The reference profile is a mixing-line structure (see Betts (1983, 1986)), joining the (conserved) saturation points (p^*, θ) of all mixtures of the two sources of air. Separate degrees of mixing may be assumed in the sub-cloud, cloud and inversion regions by specifying values of a parameter, $\gamma = \partial p^*/\partial p$. This allows the reference profiles of temperature and humidity to be computed for the convecting layer. The scheme currently assumes a partial mixing within the cloud layer with $\gamma = 1.0$. In the inversion layer at cloud top, the mixing is a function of the inversion strength with γ lying between 1.2 and 2.5 (see Betts and Miller (1993) for more details). Shallow convection is assumed to be non-precipitating, so that the scheme simply redistributes enthalpy, C_pT, and moisture separately in the vertical. The redistribution includes the model level immediately above the shallow cloud top.

The scheme uses a lagged, rather than an instantaneous, adjustment to the reference profile. Therefore the relaxation time has to be specified, and is not necessarily the same for deep and shallow convection, since they involve different processes. For deep convection the adjustment time-scale must be sufficiently short to prevent grid-scale saturation in convective situations. Resolved ascent (descent) acts to decrease (increase) the subsaturation, and the rate at which this occurs is resolution dependent. Hence, the relaxation time-scale is also resolution dependent. For the integrations described in this paper relaxation times of 2 hours for deep convection and 4 hours for shallow convection are used.

As with the Kuo scheme, deep convective cloud amounts, determined from the precipitation rate (Slingo 1987), are calculated by the scheme and passed to the radiation parametrization. A simple parametrization of shallow, non-precipitating cloud amount

is also included in the scheme, in contrast to the shallow-convection scheme used with the Kuo scheme where no cloud amounts are computed. In the adjustment scheme the shallow cumulus cloud cover is related to the moisture tendencies within the cloud layer, and gives amounts of near 30%, typically.

4. Integrations

Perpetual January integrations were performed with each version of the convective parametrization. The integrations were 360 days in length, sufficient to give a reasonable description of the intraseasonal variability. History files were kept every 6 hours so that the diurnal cycle in convection could be identified.

Initial conditions were based on the ECMWF analysis for 12 GMT on 15 January 1987. Sea surface temperatures for January, averaged over the 10 years 1979 to 1988, were used. These were based on the climatology provided for the Atmospheric Model Intercomparison Project (AMIP; Gates 1992).

5. Mean circulation and diabatic heating

The global mean energy budget and hydrological cycle averaged over the 360 days from each integration are shown in Tables 3 to 5. The energy budget of the complete earth/atmosphere system, given by the radiation budget at the top of the atmosphere (Table 3), shows that, compared with climatological estimates of 234 $W\,m^{-2}$ for the outgoing long-wave radiation (OLR) and 244 $W\,m^{-2}$ for the short-wave absorption (Slingo and Slingo 1991), the simulation with BM93 has underestimated the short-wave heating. This is primarily due to increased low-level cloudiness over the subtropical oceans as a result of the additional parametrization of trade-wind cumulus cloud amounts with the BM93 scheme (see section 3(b)). These cloud amounts tend to be too high and so further tuning of this parametrization is planned.

The global mean hydrological cycle (Table 4) is quite similar with both convection schemes. The BM93 integration has a slightly more vigorous cycle, the increased convective activity being consistent with the increased atmospheric radiative cooling shown in Table 5. The Kuo integration reaches equilibrium with a slightly drier atmosphere, as indicated by the global mean total column moisture at day 360 (Table 4), which can be compared with the initial value of 24.2 cm. Most of the drying in the Kuo integration takes place within the first 60 days.

Table 5 shows the main terms in the budget of the total potential energy of the atmosphere. As already noted, the net radiative cooling increased with BM93 and, although this is balanced in part by increased latent-heat release, there is also a substantial increase in sensible-heat flux. This occurs both in the subtropics associated with stronger trade winds with BM93, and in the eastern portions of the North Atlantic and Pacific storm tracks.

In both the hydrological and atmospheric energy budgets (Tables 4 and 5), residuals exist because of spurious sources and sinks within the model calculations. These include the non-conservative treatment of lateral dissipation, implied diffusion in the flux-limited vertical-advection scheme, the spurious source of moisture associated with filling of negative humidities, and approximations in the energy conservation in the convection schemes.

Despite similar global mean budgets the distribution of diabatic heating, both horizontally and vertically, is markedly different with the two convection schemes. Figure 1 shows vertical cross-sections of the zonal mean temperature and moisture

TABLE 3. GLOBAL MEAN ENERGY BUDGET, DAYS 0–360

	Kuo scheme	Betts and Miller (1993) scheme
Outgoing long-wave radiation (W m^{-2})	233.7	236.6
Absorbed short-wave radiation (W m^{-2})	247.5	235.7
Total cloud amount (%)	51	58

TABLE 4. GLOBAL MEAN HYDROLOGICAL CYCLE, DAYS 0–360

	Kuo scheme	Betts and Miller (1993) scheme
Convective precipitation (mm day^{-1})	2.13	2.20
Large-scale precipitation (mm day^{-1})	0.81	0.81
Surface evaporation (mm day^{-1})	2.87	2.95
Total column moisture at day 360 (mm)	22.6	24.0

TABLE 5. GLOBAL MEAN ATMOSPHERIC TOTAL POTENTIAL ENERGY BUDGET (W m^{-2}), DAYS 0–360

	Kuo scheme	Betts and Miller (1993) scheme
Short-wave heating	69.2	71.9
Long-wave cooling	171.8	184.3
Net radiative cooling	102.6	112.4
Latent-heat release	85.1	87.0
Surface sensible-heat flux	18.3	24.2

tendencies due to convective processes (shallow and deep) and to all diabatic processes (i.e. convection, radiation, vertical diffusion, large-scale precipitation) averaged over days 60.25 to 360 from both integrations. With the Kuo scheme the latitudinal extent of the deep convective heating (Fig. 1(a)) is very broad, with the maximum heating in the lower troposphere. In contrast the BM93 scheme has simulated a very well defined region of deep equatorial heating (Fig. 1(e)), with maximum values extending into the upper troposphere. The deeper heating with the BM93 scheme is in better agreement with estimates of the heat source due to large-scale convection, Q_1, based on observations (e.g. Yanai *et al.* 1973; Tiedtke 1989). The negative values near the tropopause with the BM93 scheme are the result of the energy correction, described in section 3(b), although small cooling tendencies are also possible from convective overshoot. These cooling tendencies are compensated for by the radiation tendencies, so that the total diabatic heating near the tropopause is small (Fig. 1(g)). There are also substantial differences in the convective heating in the northern hemisphere middle latitudes which, although outside the scope of this paper, appear to have had a substantial impact on the extra-tropical transient circulation. Research into this aspect of the model's sensitivity to convective parametrization is continuing.

The moisture tendencies due to convective processes (Figs. 1(b) and 1(f)) show substantial drying of the boundary layer, which is compensated for by moistening due to surface evaporation and vertical diffusion. The total moisture tendencies due to all diabatic processes (Figs. 1(d) and 1(h)) show a moistening of the lower troposphere in the subtropics and tropics in the region of the trades. This moisture is transported equatorwards by the low-level flow and supports the precipitation of the ITCZ. In the deep tropics both schemes show drying tendencies, which extend much higher in the

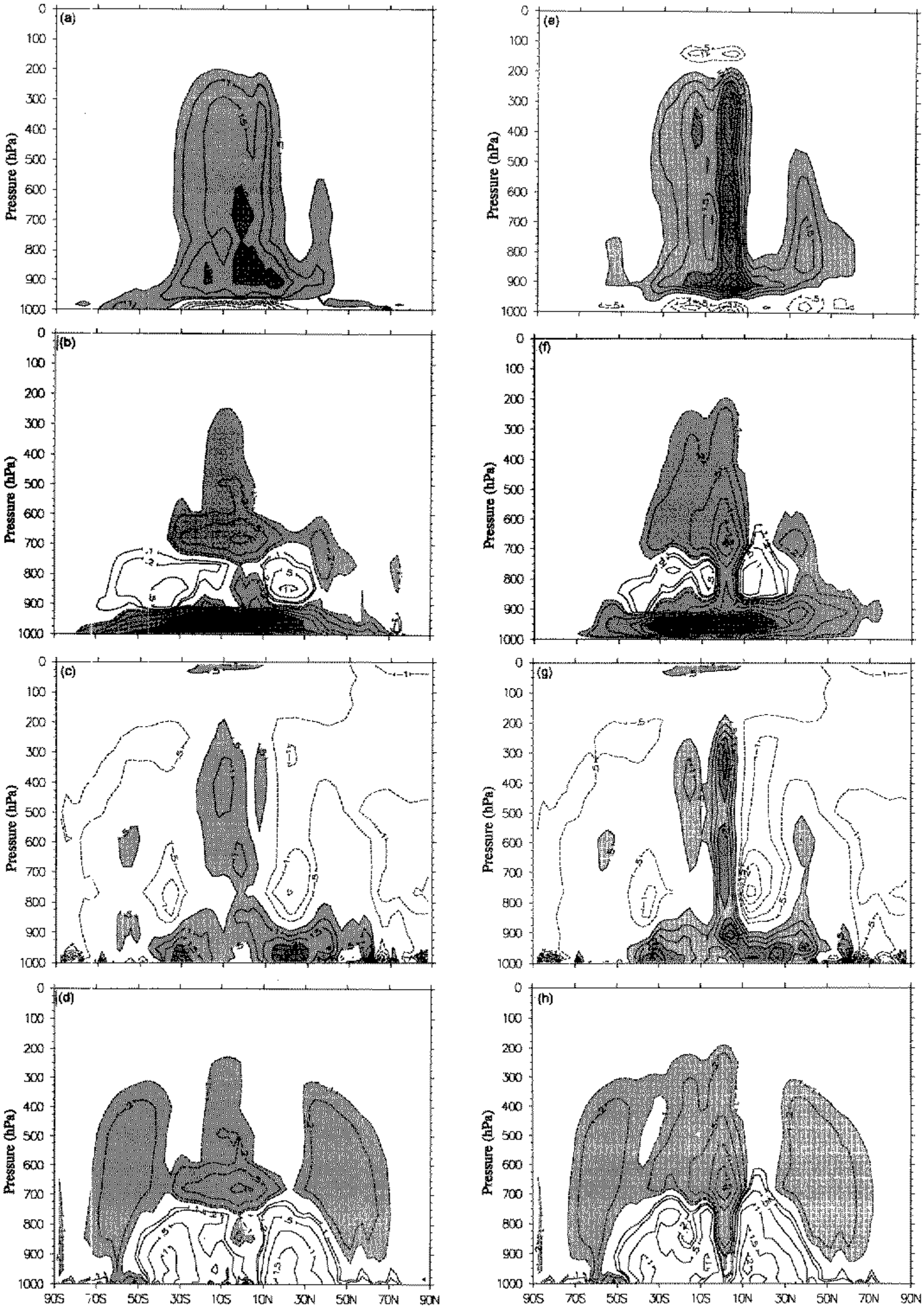

Figure 1. Zonal mean cross-sections of convective and total diabatic temperature (contour interval 0.5 K day^{-1}) and moisture (contours at 0.1, 0.2, 0.5, 1.0 and 1.5 g kg^{-1} day^{-1}) tendencies, averaged over days 60.25 to 360. (a) Convective temperature, (b) convective moisture, (c) total diabatic temperature, and (d) total diabatic moisture, from the Kuo scheme; (e)–(h) are as (a)–(d), but for the Betts and Miller (1993) scheme. No zero contours are drawn and negative contours are dashed. Shading denotes heating and drying respectively.

troposphere with the BM93 scheme. Again the greater vertical extent of the drying with the BM93 scheme is in better agreement with estimates of the moisture sink, Q_2, based on observations (e.g. Yanai *et al.* 1973; Tiedtke 1989).

As expected from the heating profiles shown in Fig. 1, the mean meridional circulation simulated with the BM93 scheme is considerably more intense (Fig. 2). The ascending branch of the Hadley circulation is more locally confined near the equator with the descending branch near 20°N. The northern hemisphere Ferrel cell is somewhat weaker with the BM93 scheme, consistent with the increased heating near 35°N. Comparison with global circulation diagnostics based on the ECMWF analyses (Hoskins *et al.* 1989) suggests that the mean meridional circulation simulated by the BM93 scheme is too intense. However, verification of this field is difficult, mainly because data from numerical weather-prediction (NWP) analyses are heavily influenced by the first-guess field in the tropics and, therefore, reflect the characteristics of the physical parametrizations within the forecast model, particularly the convection scheme.

The thermodynamic structures simulated by both versions of the model have been verified by comparing them with radiosonde observations of temperature and specific

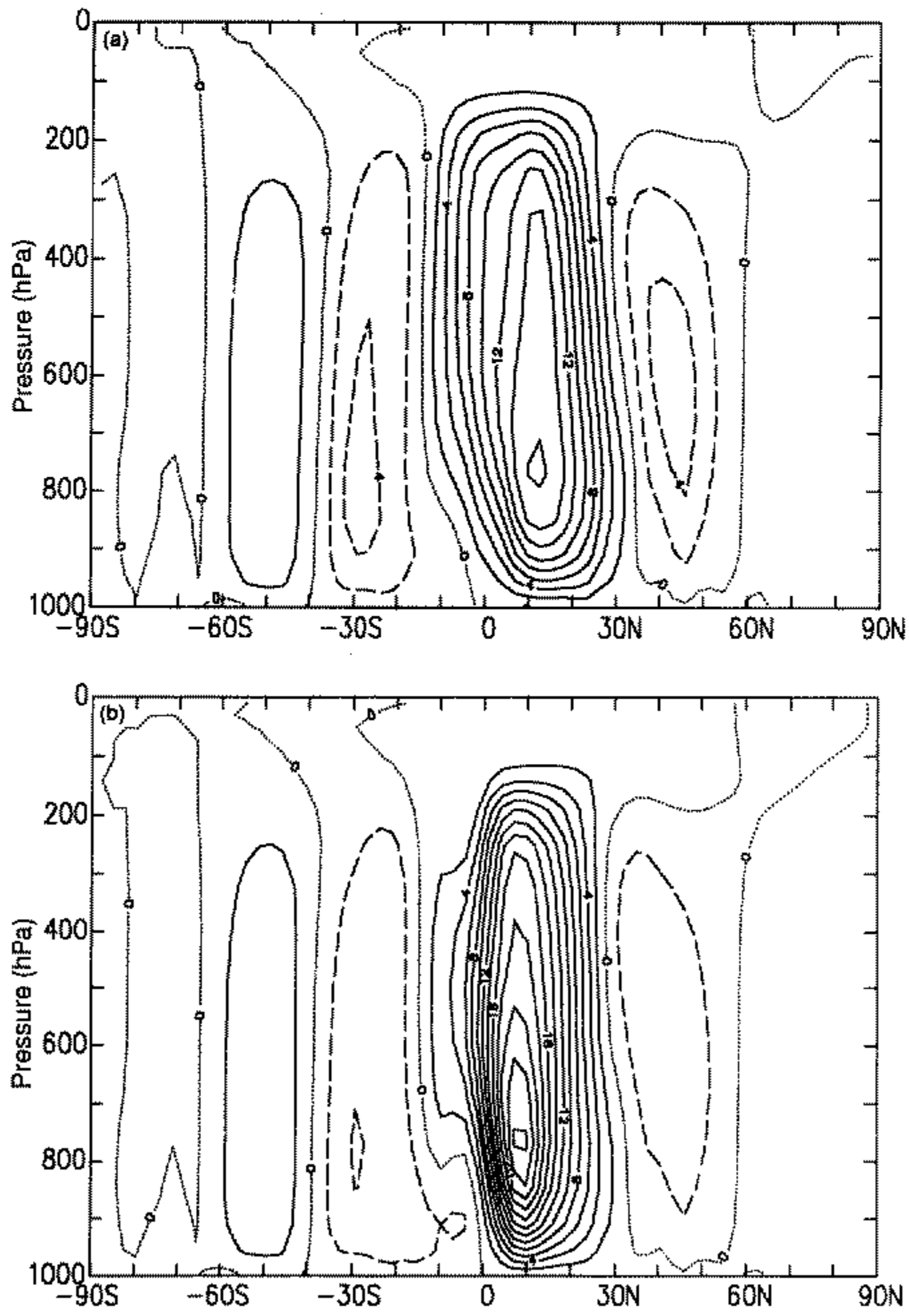

Figure 2. Mean meridional circulation (kg s^{-1}) averaged over days 60.25 to 360 with (a) the Kuo scheme, and (b) the Betts and Miller (1993) scheme. The contour interval is 2×10^{10} kg s^{-1}, and negative contours are dashed.

humidity from a number of stations throughout the tropics and subtropics. These observations have been compiled from rawinsonde reports for January, covering the period beween about 1960 and the late 1980s, and were made available by Bruce Briegleb, National Center for Atmospheric Research (personal communication). They have proved particularly useful for verifying the model's humidity distribution since this field is not well represented by NWP analyses.

In the deep tropics both convection schemes produce very good temperature profiles, with differences from observations of the order of 1 K, within the standard deviation of the observations. This agreement is despite very substantial differences in the diabatic heating profiles and the mean meridional circulation. Figure 3(a) shows such an example for Truk Island (7°N, 151°E) in the west Pacific, where the model data are from the time mean for the last 60 days of each integration. The main difference between the two integrations occurs in the lower troposphere, where the Kuo scheme overestimates the strength of the weak inversion whilst the BM93 scheme underestimates it. The model's humidity distribution differs substantially in convective regions (Fig. 3(b)). The Kuo scheme consistently dries the troposphere above 750 hPa whilst the BM93 scheme tends to simulate a boundary layer which is slightly too moist. The humidity errors with the Kuo scheme mean that the static stability, as measured by the vertical gradient of equivalent potential temperature, is poorly represented in the lower and middle troposphere (Fig. 3(c)).

In the subtropics neither simulation has been as successful in simulating the temperature structure. Typical warm biases of about 3 K are obtained, as can be seen in the comparison for Midway Island (28°N, 183°E) in the north Pacific (Fig. 4(a)). In this region the temperature structure is largely determined by adiabatic warming, associated with subsidence, and radiative cooling. Both integrations also simulate humidity profiles

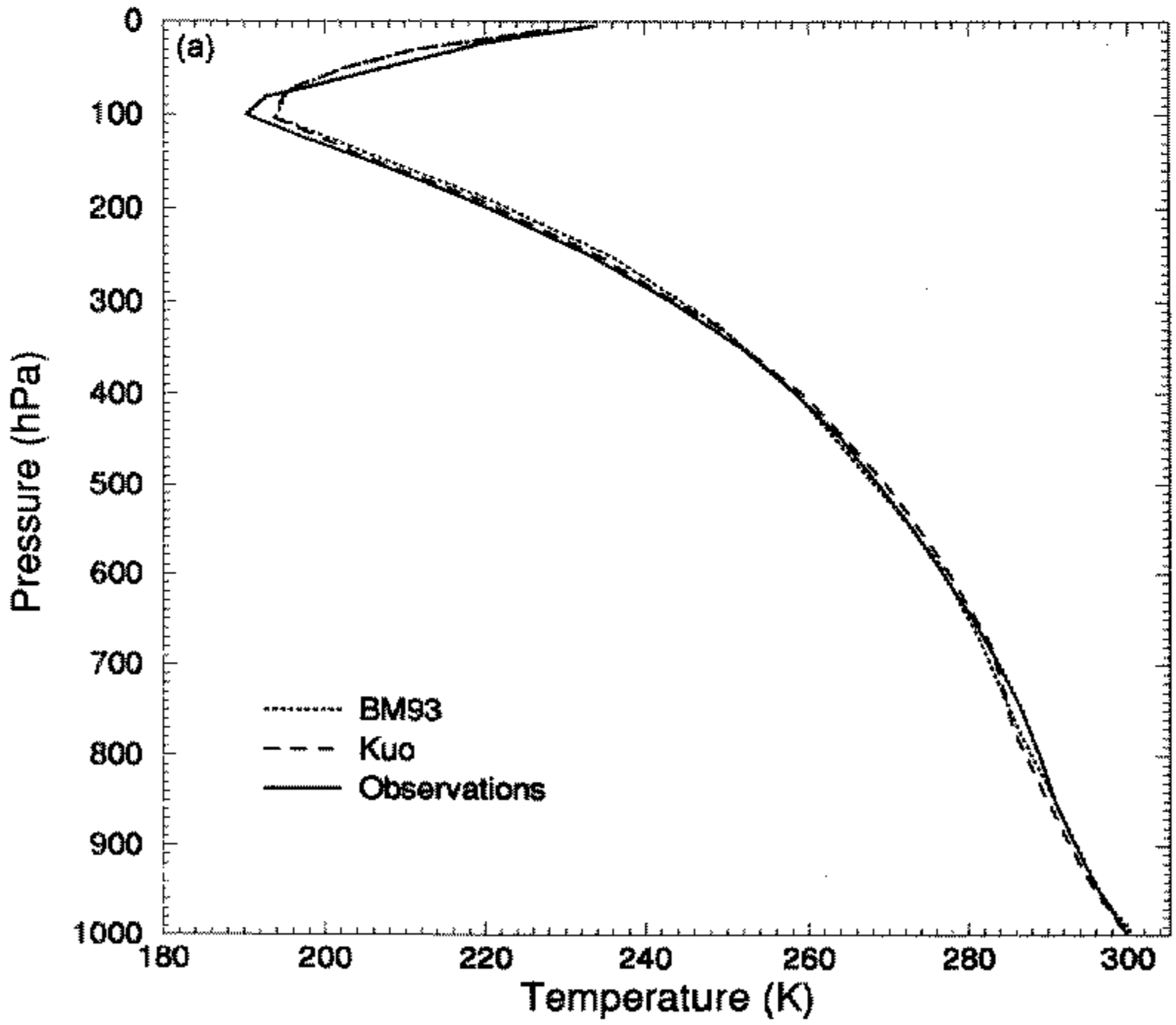

Figure 3. Vertical profiles of (a) temperature, (b) specific humidity, and (c) equivalent potential temperature from both schemes (averaged over days 300.25 to 360), and from radiosonde observations for Truk Island in the west Pacific.

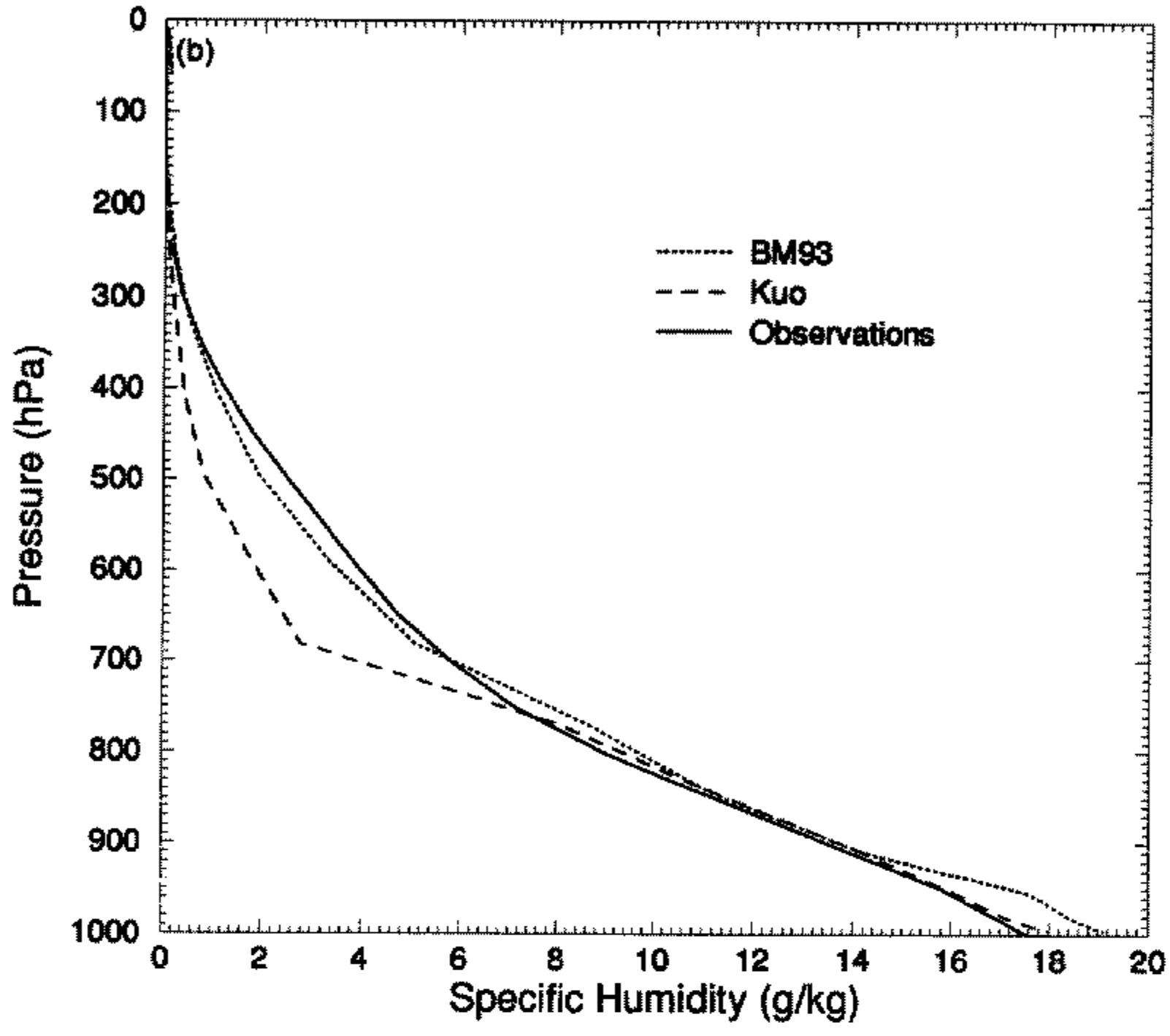

Figure 3. Continued.

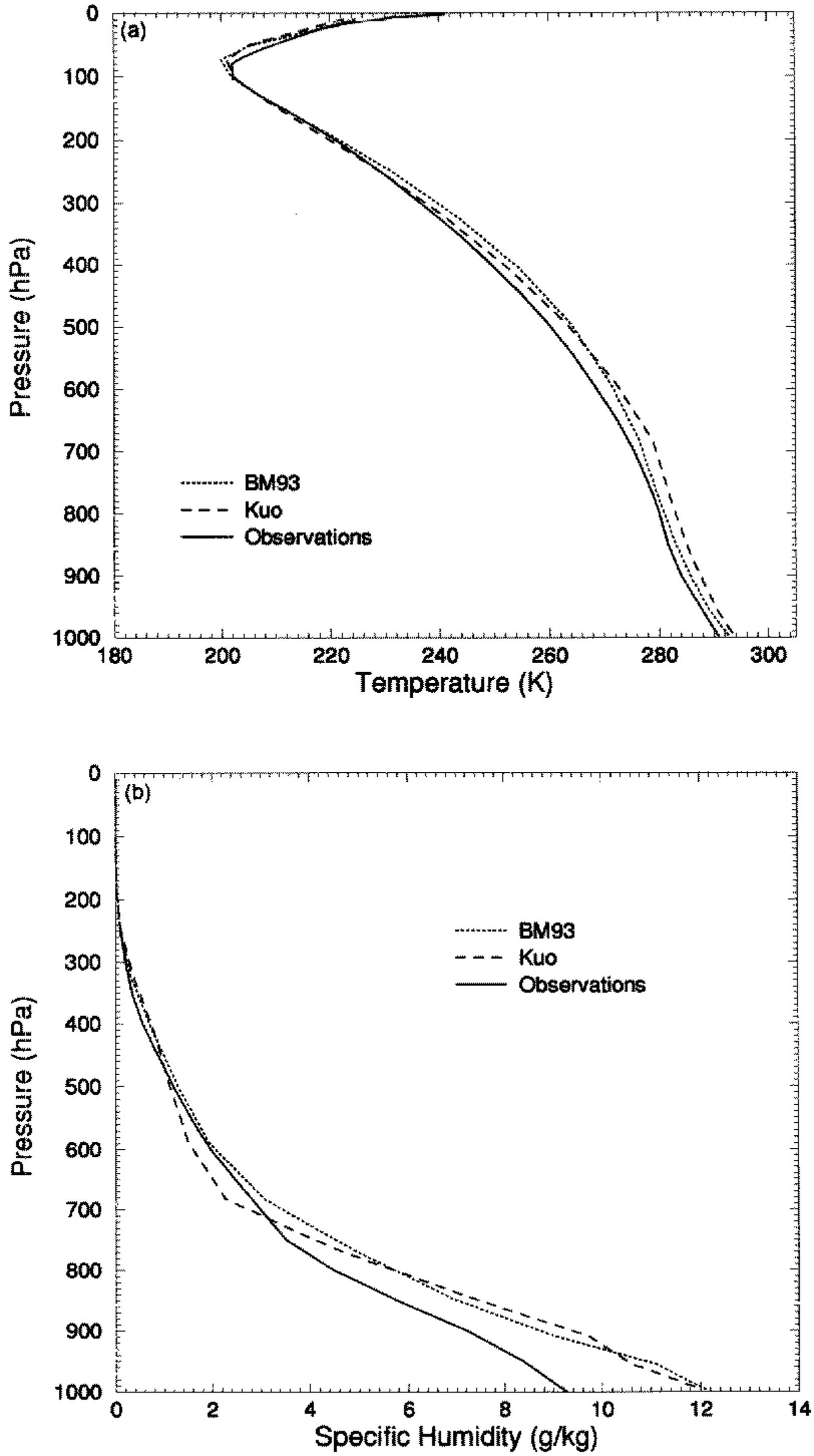

Figure 4. Vertical profiles of (a) temperature, and (b) specific humidity from both schemes (averaged over days 300.25 to 360), and from radiosonde observations, for Midway Island in the North Pacific.

that are consistently too moist by a substantial amount near the surface (Fig. 4(b)). Thus, θ_e is too high at all tropospheric levels, although its gradient is represented reasonably well. This can be seen in Fig. 5 where the profiles of θ_e from the observations and from the integration with the BM93 scheme are compared for Truk Island and Midway Island. The transition from a deep unstable layer over Truk Island to a much more stable profile over Midway Island has been successfully captured with the BM93 scheme.

The vertical cross-sections of the zonal mean u-wind components from both integrations and from the ECMWF analyses for 1983 to 1989, as processed by the Joint Diagnostics Project (Hoskins *et al.* 1989), are shown in Fig. 6. Although the strength of the subtropical jets is simulated reasonably well, both versions of the model have positioned the southern hemisphere jet too far polewards. In the tropics, the upper-level easterlies are too strong, particularly with the Kuo scheme, and the transition region between easterly and westerly winds is too far polewards in both simulations.

Despite global mean budgets which suggest that, in gross terms, the two schemes give similar results, regional differences are already apparent in zonally averaged fields. They are even more evident in the latitude–longitude pictures of the time-mean convective precipitation (mm day^{-1}) from each convection scheme, given in Fig. 7. The Kuo scheme produces a rather diffuse structure to the ITCZ, particularly in the west Pacific (Fig. 7(a)), with extensive areas of weak precipitation. In contrast the BM93 scheme produces a quite narrow and intense ITCZ, with the strongest precipitation being concentrated over the warm-pool region of Indonesia and the west Pacific (Fig. 7(b)). The increased convective rainfall in the growth regions of the northern hemisphere storm tracks with the BM93 scheme can also be seen. The rather narrow structure to the ITCZ with the BM93 scheme may be a result of running the model in perpetual mode, which allows the precipitation zone to become locked in one position, but preliminary results

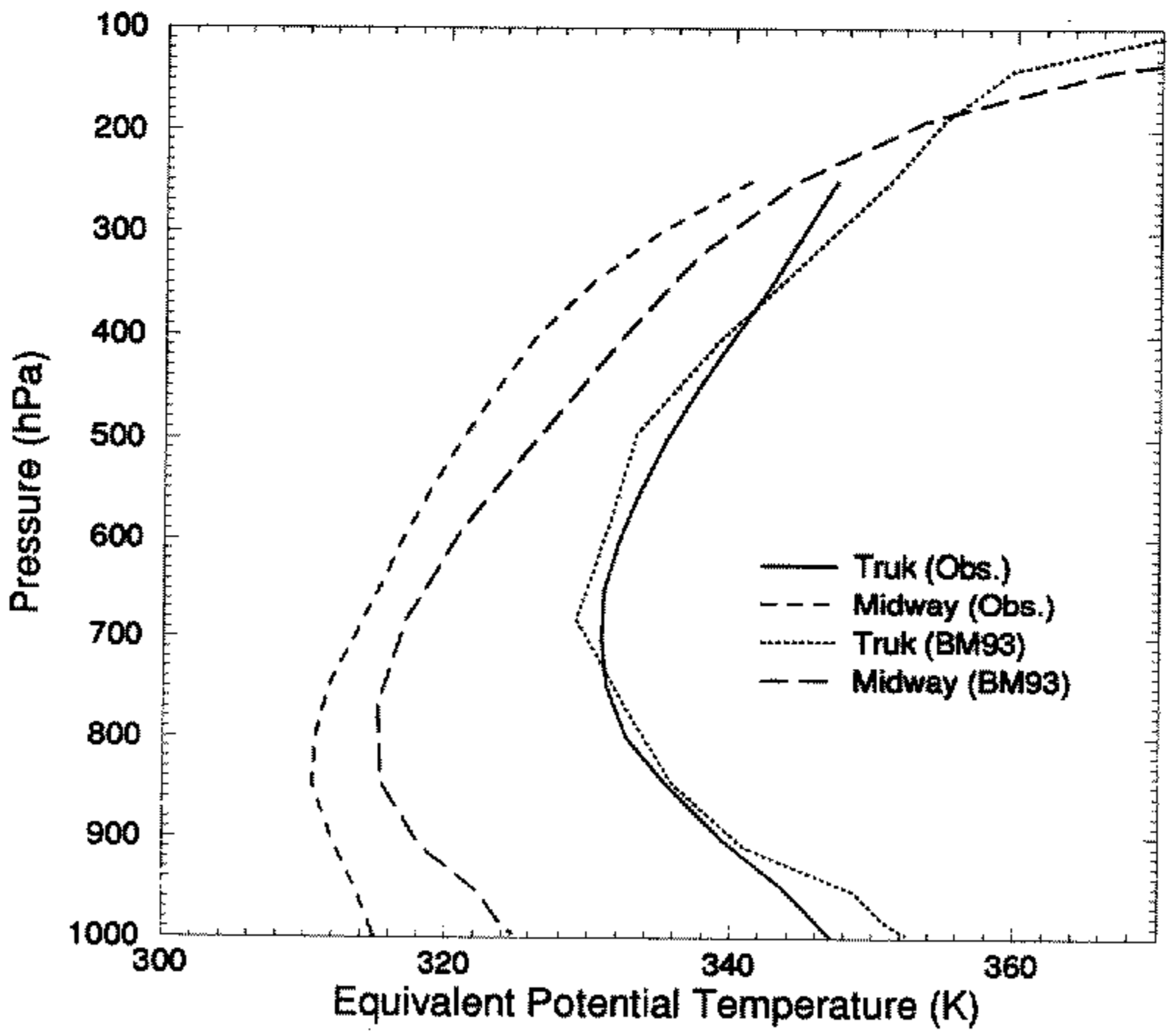

Figure 5. Comparison of the vertical profiles of equivalent potential temperature for Truk Island and Midway Island, as observed from radiosondes and as simulated for days 300.25 to 360 with the Betts and Miller (1993) scheme.

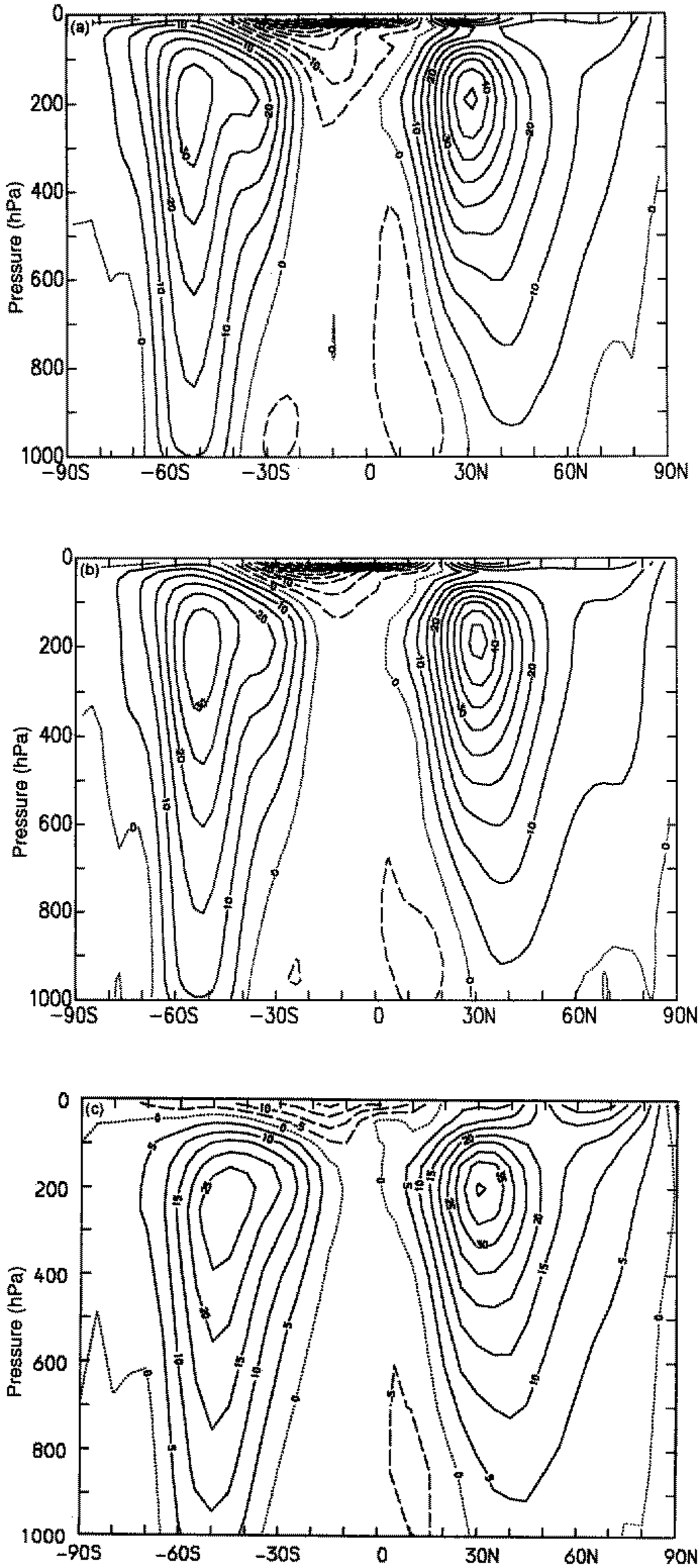

Figure 6. Vertical cross-sections of the mean zonal wind component ($m\,s^{-1}$) from (a) the Kuo scheme, (b) the Betts and Miller (1993) scheme, and (c) the ECMWF analyses. The model data are averaged over days 60.25 to 360. The contour interval is $5\,m\,s^{-1}$ and negative contours are dashed.

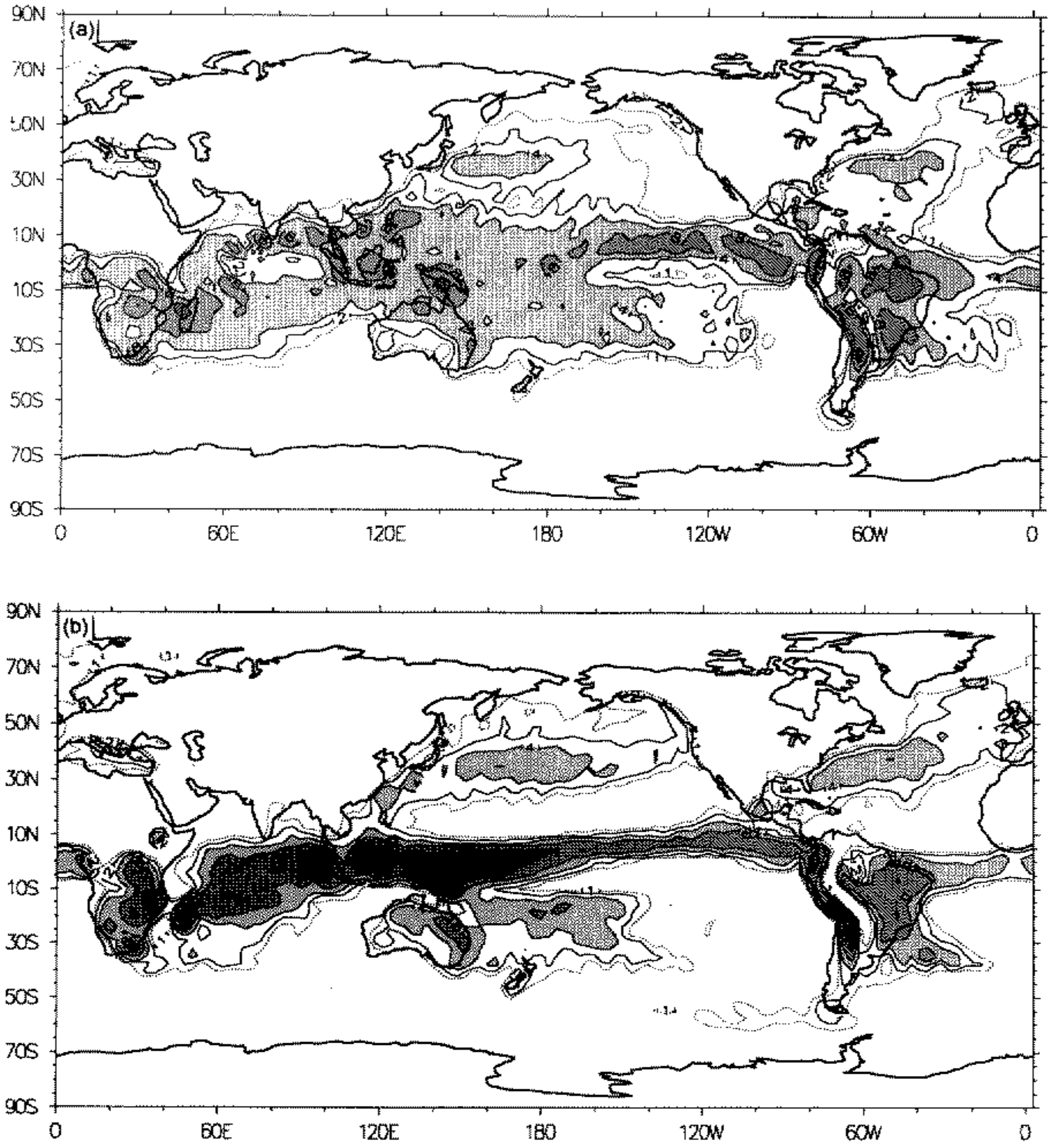

Figure 7. Mean convective precipitation (mm day^{-1}) for days 60.25 to 360 from (a) the Kuo scheme and (b) the Betts and Miller (1993) scheme. The dotted contour is 1 mm day^{-1}; solid contours are at 2, 4, 8, 16 and 32 mm day^{-1}. Light shading is used between 4 and 8 mm day^{-1}, medium shading between 8 and 16 mm day^{-1} and dark shading for values in excess of 16 mm day^{-1}.

from a multi-seasonal cycle integration suggest that this is a characteristic of the scheme. The precipitation rates simulated in the ITCZ by the BM93 scheme appear to be stronger than suggested by available climatologies, but considerable differences exist between the various observed estimates (e.g. Spencer 1993).

Figure 8 shows the time-mean distribution of the OLR for the tropical belt, simulated by both versions of the model, and observed by the Earth Radiation Budget Experiment (ERBE) for January 1986. The minima are associated with cold, deep clouds and, in the tropics, are good indicators of precipitation. Both versions of the model show the main areas of low OLR over the west Pacific, South America and South Africa, as observed (Fig. 8(c)). Superimposed on the distributions of OLR shown in Fig. 8 are isopleths of the SSTs. The observed OLR shows a clear correspondence between warm SST and low OLR (or high precipitation). The tendency for deep convection to fall within the 28 °C SST isotherm, as evident in the ERBE data, has been widely observed, although no satisfactory explanation exists to explain this association (e.g. Webster 1990). Both

versions of the model shows a corresponence between warm SSTs, low OLR and hence convective activity. However, Fig. 8(b) suggests that the BM93 scheme underestimates the convection south of the equator, associated with the South Pacific Convergence Zone (SPCZ), whilst producing a too intense ITCZ north of the equator.

As expected from the simulations of the distribution of diabatic heating implied by Figs. 7 and 8, the planetary-scale divergent circulation is quite well represented by both versions of the model when compared with that derived from ECMWF analyses for the years from 1980 to 1987 (Fig. 9). The Walker circulation (implied by the gradient from the west to the east Pacific) appears to be somewhat overestimated in the model. However, the climatological estimates of velocity potential, based on NWP analyses, are extremely sensitive to the physical processes used within the forecast model which forms the basis of the analyses, and should therefore be treated with caution. In addition, comparing a single vertical level can be misleading, since the vertical structure of the velocity potential may be quite complicated in the upper troposphere, due to varying heights for the outflow levels of deep convection.

As noted earlier in section 2(b) the ability of the model to simulate the upper-level westerlies in the equatorial central and east Pacific is crucial for the interaction of the tropics with the extratropics. The simulation of these westerlies has been shown to be closely linked to the strength of the diabatic heating over the warm pool of the west Pacific and Indonesia, both in idealized studies (Sardeshmukh and Hoskins 1988) and from GCM results (see section 2(b)). The upper tropospheric zonal wind component is simulated reasonably well by both versions of the model in comparison with ECMWF analyses (Fig. 10). The BM93 scheme gives a more realistic simulation of the equatorial westerlies in the east Pacific, but both versions of the model still display an equatorial easterly bias. Over South America this is related to an anomalous upper tropospheric anticyclonic circulation driven by the excessive heating over the Andes. The simulation of the northern hemisphere mid-latitude jets is satisfactory, although the Pacific jet extends too far east and north in both integrations.

Figure 11 shows the winds at 850 hPa for the tropics between 30°N and 30°S from both versions of the model and from ECMWF analyses. With the Kuo scheme the winds lack a meridional component in both the Pacific and Atlantic Oceans. Hence the pronounced convergence over the equatorial west Pacific, associated with the winter monsoon, is rather weak with the Kuo scheme but simulated quite well with the BM93 scheme. However, in the time mean, the westerly flow to the north of Australia into the SPCZ is better simulated with the Kuo scheme, although the BM93 scheme produces periods of strong westerlies during the integration.

In summary, both versions of the model have produced viable simulations of the time-mean circulation over the tropics. They differ in detail, but it would be hard to say that either was superior, bearing in mind the uncertainty in the verification analyses (particularly as the tropical oceans are data sparse) and the fact that the satellite data used in Fig. 8(c) are for one specific year.

6. Transient characteristics

(*a*) *Total transience*

Although both integrations produce reasonable simulations of the tropical time-mean climate, their transient characteristics are markedly different. Figure 12 shows the total variance of the OLR from both integrations. Again, isopleths of SST have been superimposed to show how well the variability in the convective activity is correlated with the SST.

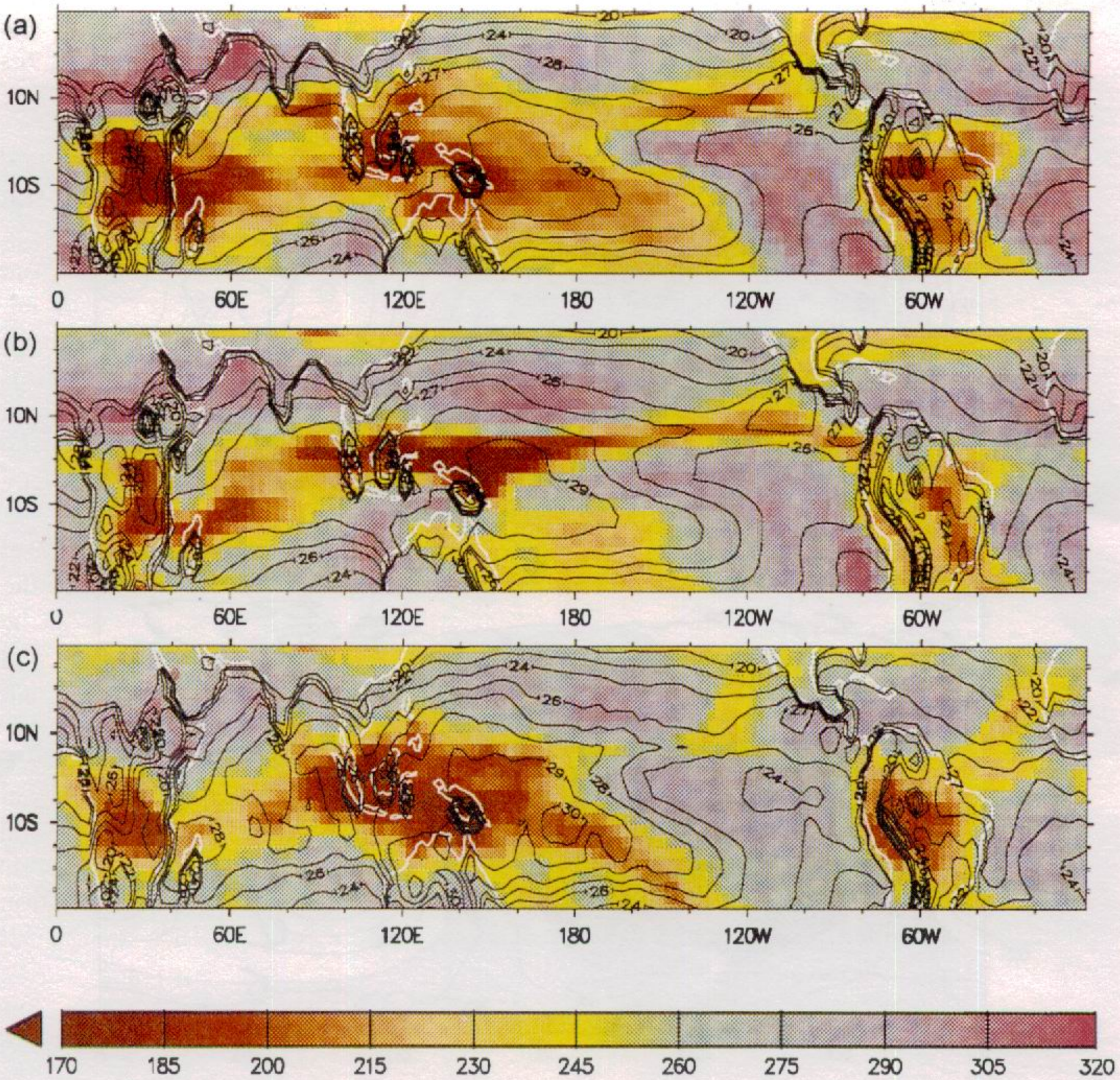

Figure 8. Mean outgoing long-wave radiation (colour scale; W m^{-2}) and sea surface temperature (contours; K) for (a) the Kuo scheme, (b) the Betts and Miller (1993) scheme and (c) observed for January 1986 from the Earth Radiation Budget Experiment. Actual sea surface temperatures for January 1986 are used in (c). The model fields are averaged over days 60.25 to 360.

In a study of satellite data, Salby *et al.* (1991) noted that convectively active regions of the tropics, characterized by low OLR, are also regions where the variance is high. As with the time-mean OLR, the variance of the convective activity has been observed to be well correlated with warm SSTs (Webster and Lukas 1992). For comparison with the model results, Fig. 13 shows the time mean and variance of the brightness temperature as observed by satellites for December, January and February 1983/84 (Hendon, personal communication). These figures were produced from the Global Cloud Imagery, developed by Salby *et al.* (1991) from data of the International Satellite Cloud Climatology Project (ISCCP). It is clear from a comparison of Figs. 8, 12 and 13 that the Kuo scheme (Fig. 12(a)) shows a poor correspondence between regions of low OLR and high transience. In fact the area of greatest transience lies over the east Pacific and appears to be associated with incursions of extratropical troughs. Over the warm pool the Kuo scheme has lower variability, suggesting that the diabatic heating in this region is

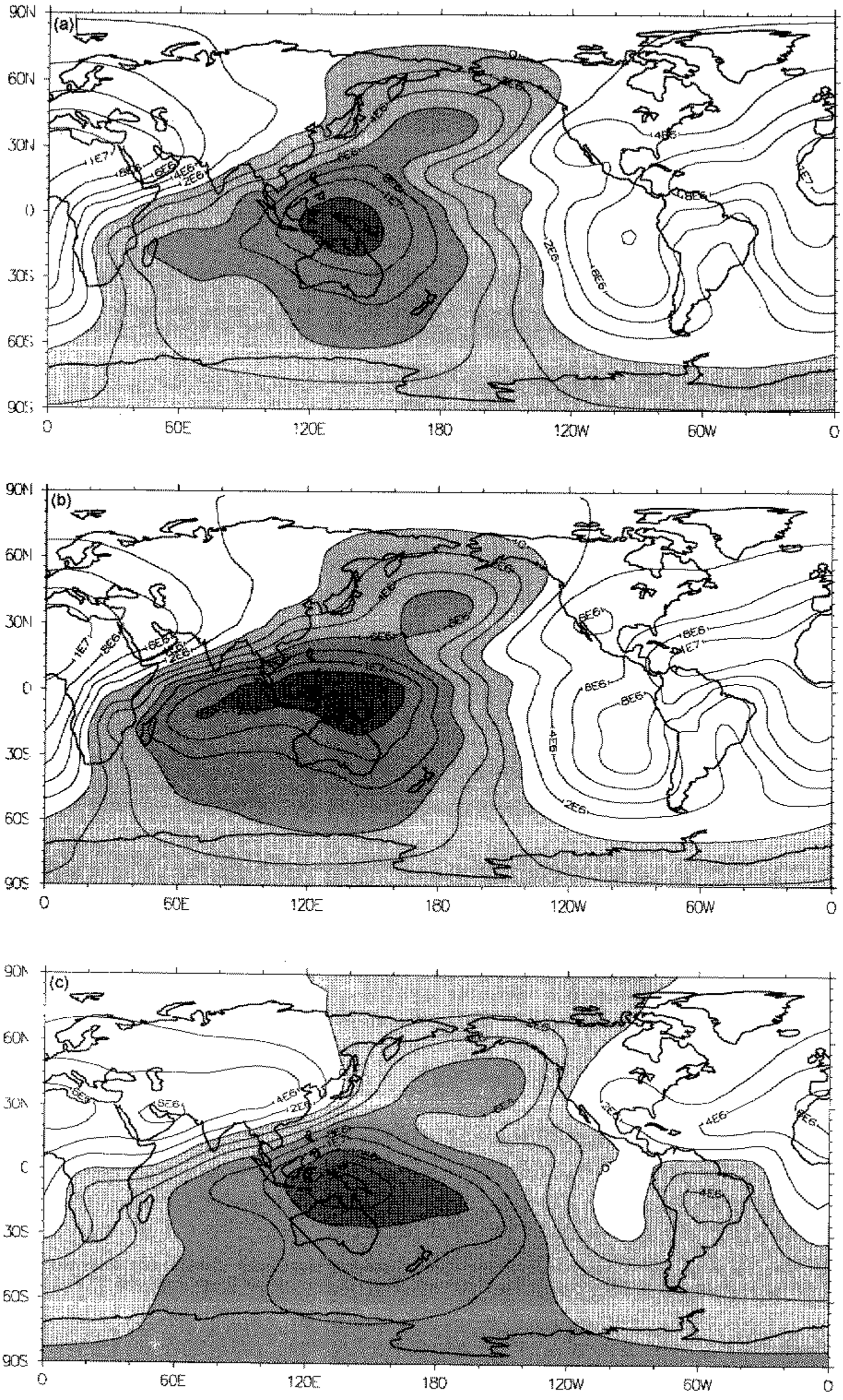

Figure 9. Mean velocity potential ($m^2\,s^{-1}$) at 200 hPa from (a) the Kuo scheme, (b) the Betts and Miller (1993) scheme, and (c) the ECMWF analyses. The model data are averaged over days 60.25 to 360. The contour interval is $2 \times 10^6\,m^2\,s^{-1}$ and negative values are shaded.

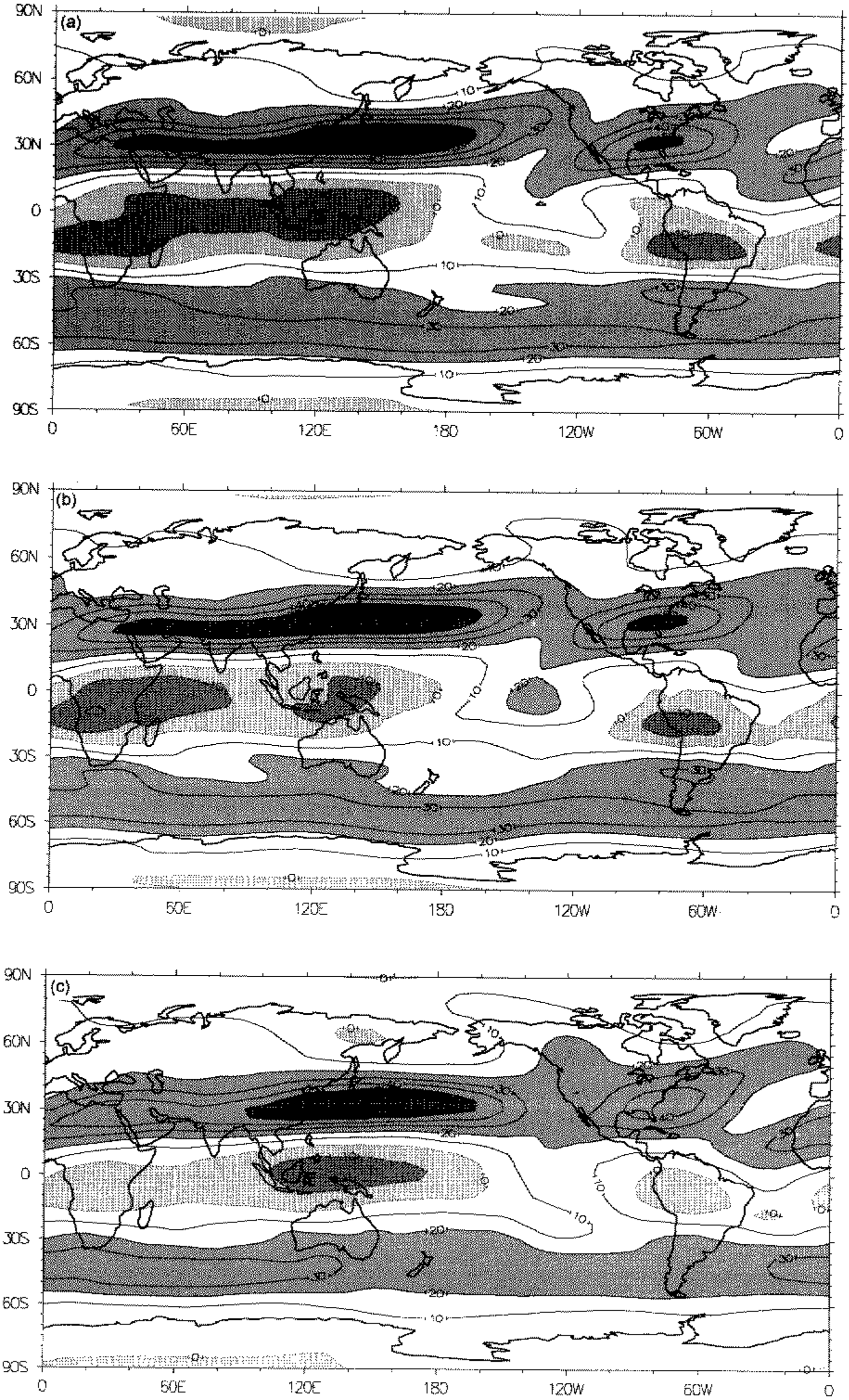

Figure 10. Mean zonal wind component ($m\ s^{-1}$) at 200 hPa from (a) the Kuo scheme, (b) the Betts and Miller (1993) scheme, and (c) the ECMWF analyses. The model data are averaged over days 60.25 to 360. The contour interval is $10\ m\ s^{-1}$ and negative values are dashed.

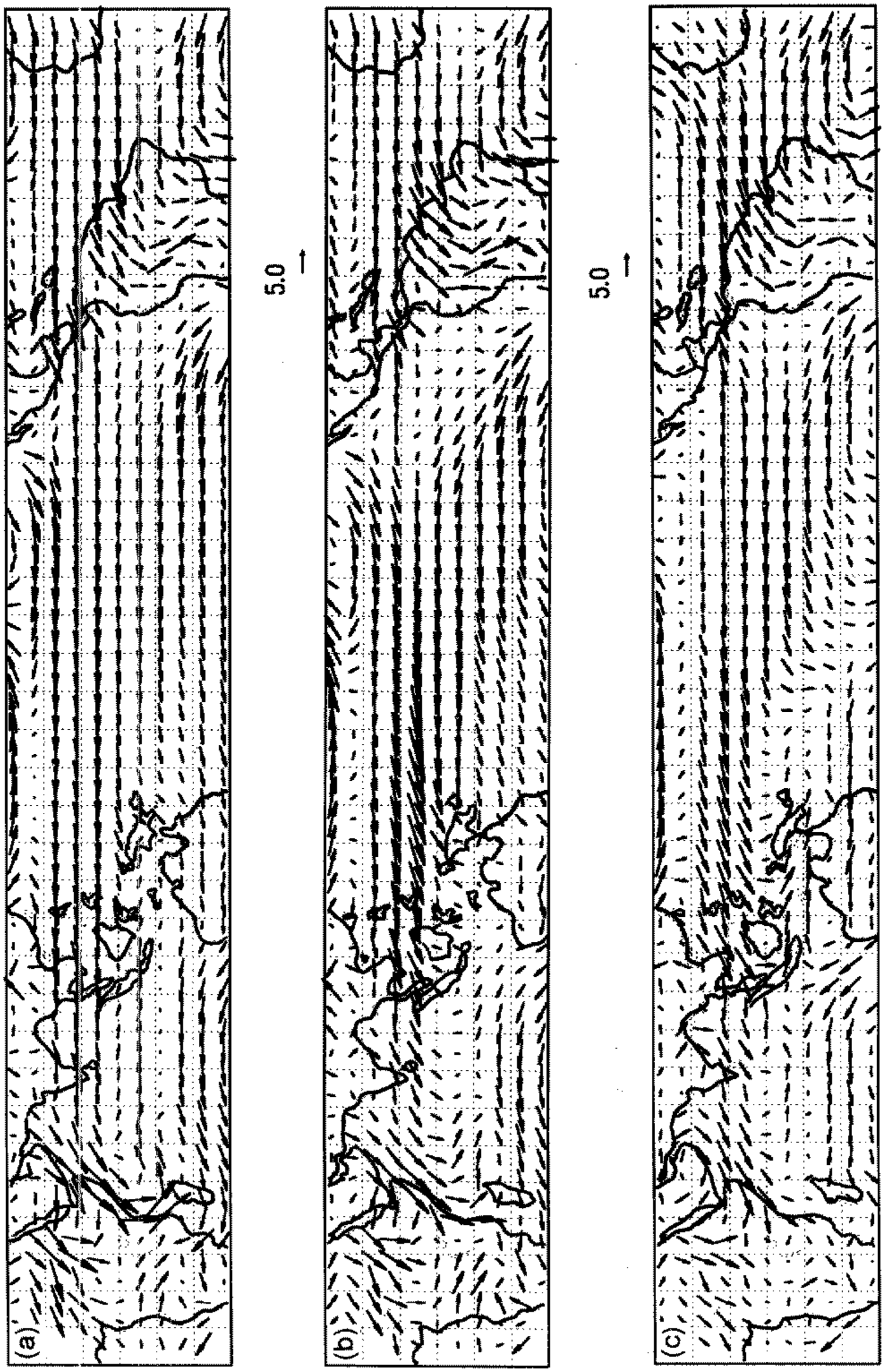

Figure 11. Mean winds at 850 hPa for the tropical belt, 30°N to 30°S, from (a) the Kuo scheme, (b) the Betts and Miller (1993) scheme, and (c) the ECMWF analyses. The model data are averaged over days 60.25 to 360.

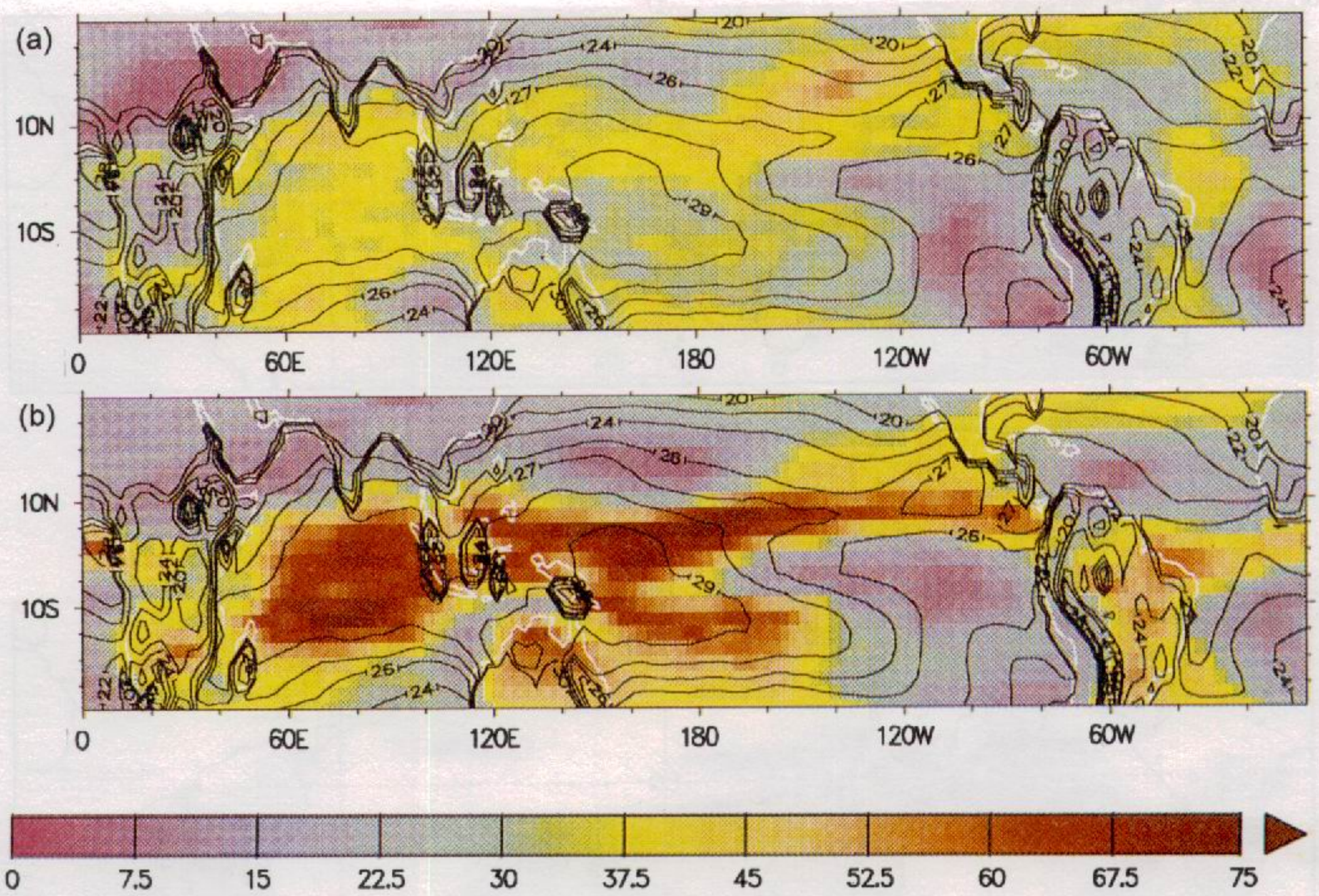

Figure 12. Square root of the total transience of the outgoing long-wave radiation (colour scale; W m^{-2}), and the time-mean sea surface temperature (contours; K) for (a) the Kuo scheme, and (b) the Betts and Miller (1993) scheme. The model fields are averaged over days 60.25 to 360.

associated with fairly continuous precipitation. The correlation of the transience with warm SSTs is demonstrably weak in this version of the model.

The BM93 scheme, on the other hand, shows a very strong relationship between the time-mean OLR, its transience and the warm SSTs (Fig. 12(b)). Consistent with satellite observations (Fig. 13 and, for example, Lau and Chan 1988; Salby *et al.* 1991), the convective variability resides predominantly over the tropical warm pool, with secondary maxima over the east Pacific and the major tropical continents. Over the Pacific the variance associated with the ITCZ and the SPCZ can be clearly identified. In contrast to the observed distribution (Fig. 13(b)), the BM93 scheme has more activity to the north of the equator in the Pacific, and relatively less variability within the SPCZ.

In terms of the magnitude of the total variance the BM93 scheme may be too active. For example, the maximum transience is considerably larger than that reported by Lau and Chan (1988) who based their results on an analysis of NOAA* satellite data, using a coarser spatial resolution of 5° latitude/longitude. Thus a direct comparison is not really possible and it is probably necessary to compare observations and model data with the same temporal and spatial sampling to draw any quantitative conclusions. However, Morcrette (personal communication) has suggested that the emissivities used for the model's cirrus clouds may be overestimated in the radiation scheme, leading to too low values of OLR in convective situations and to an overestimate of the OLR variance. Nevertheless, comparison of the *patterns* of variability shown in Figs. 12 and 13 demonstrates the differing characteristics of the two schemes, with an indication of superior results from the BM93 scheme.

* National Oceanic and Atmospheric Administration.

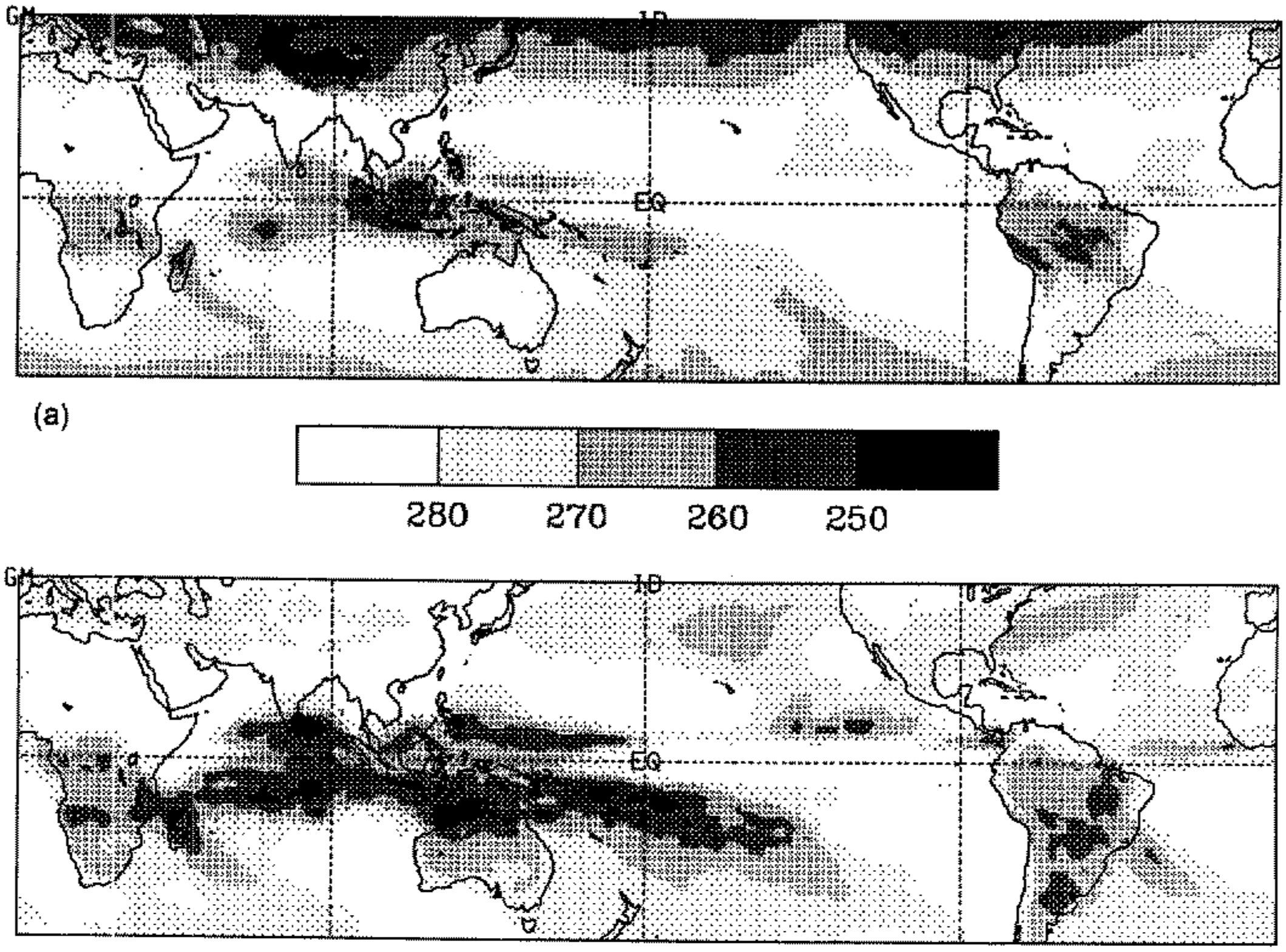

Figure 13. (a) Mean (K) and (b) total variance (K^2) of the window brightness temperature from Global Cloud Imagery data for December, January and February, 1983/84.

(*b*) *Diurnal variability*

Since the model history files were kept every 6 hours, an assessment of the diurnal behaviour of convective activity can be made. As in Slingo *et al.* (1992), the intradiurnal ($\leqslant 1$ day) variance is mostly explained by that directly linked to the response of the land/atmosphere system to the diurnal cycle in the solar radiation. To identify the coherent diurnal variability, the time-mean OLR was computed for each of the four times of day, separated by 6-hour intervals, and the standard deviation of the four means calculated. Figure 14 shows the coherent diurnal variability simulated by each convection scheme for days 60.25 to 360. These results can be compared with the amplitude of the diurnal harmonic estimated from the data of four sun synchronous satellites by Hartmann and Recker (1986). (Note that the diurnal harmonic explains over 95% of the coherent diurnal standard deviation (Slingo *et al.* 1992).)

Hartmann and Recker (1986) showed that, over the tropical oceans, the diurnal harmonic has a well-defined structure, associated with convection. Amplitudes of between 2 and 5 W m^{-2} are typical. The simulation with the Kuo scheme (Fig. 14(a)) appears to overestimate the diurnal cycle over the oceans by a considerable extent, whereas the BM93 scheme (Fig. 14(b)) has produced a more realistic response. Similarly, over the tropical land where convection occurs (typified by low values of OLR in Fig. 8), the Kuo

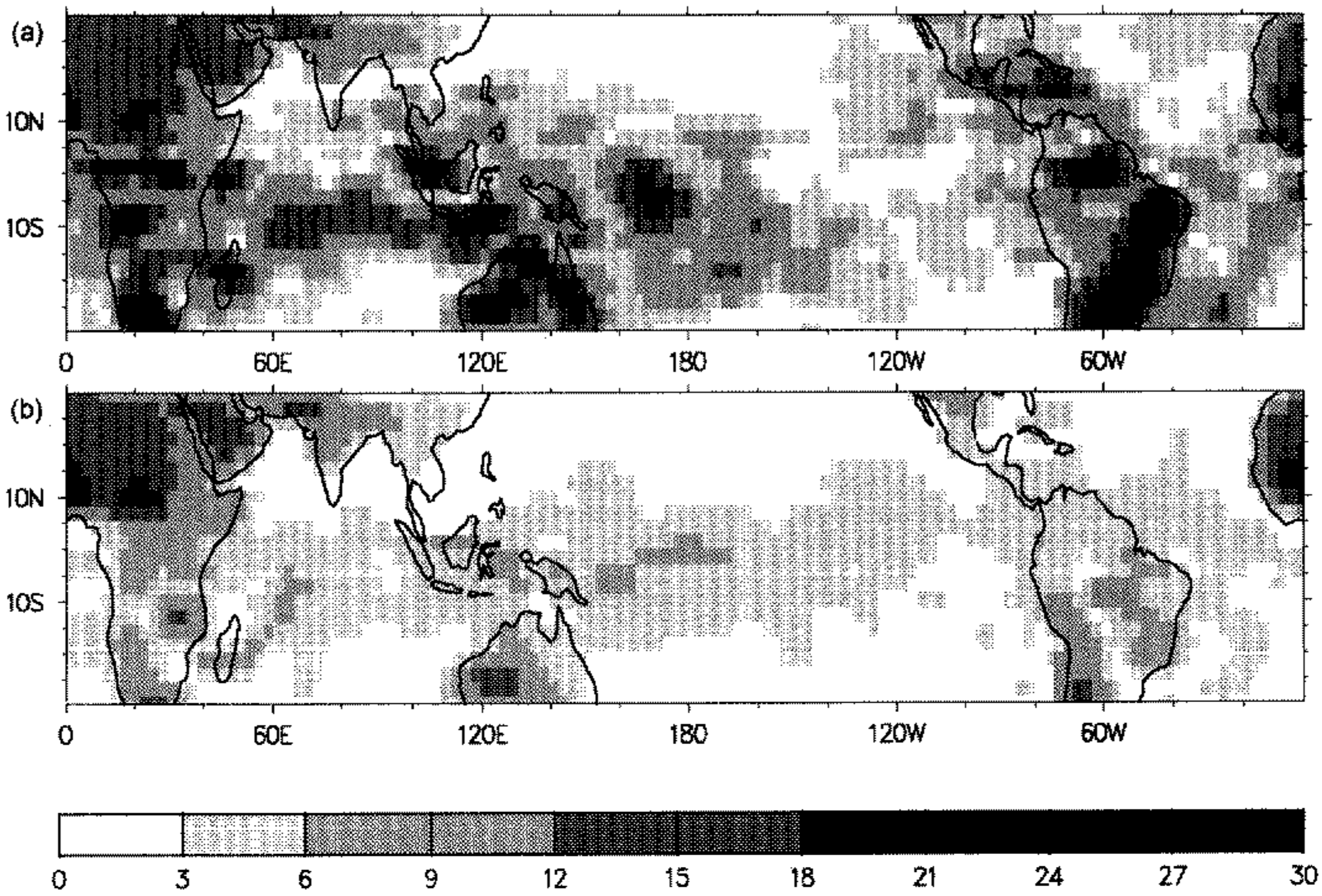

Figure 14. The amplitude of the coherent diurnal cycle ($W\,m^{-2}$) for days 60.25 to 360 from (a) the Kuo scheme, and (b) the Betts and Miller (1993) scheme.

scheme again overpredicts the diurnal amplitude, with values in excess of $20\,W\,m^{-2}$ compared with Hartmann and Recker's estimates of nearer $10\,W\,m^{-2}$.

These results suggest that the Kuo scheme has an unrealistically sensitive response to the diurnal cycle in short-wave heating. Over land this may be associated with convergent circulations being set up in the form of a large-scale sea breeze, in response to surface solar heating. Over the oceans the reason for the large diurnal cycle is less clear. It may be related to the diurnal tide (Hsu and Hoskins 1989), but the temporal sampling used in these integrations is not sufficiently good to identify the phase of the diurnal cycle. A comprehensive analysis of the diurnal cycle is planned for future research.

(c) *Interdiurnal variability*

At interdiurnal frequencies the various time-scales of simulated convective activity have been studied by decomposing the variance into synoptic (2–6 days, 6–14 days) and intraseasonal (14–30 days, 30–70 days) time-scales (Figs. 15 and 16), following Kiladis and Weickmann (1992). With the Kuo scheme (Fig. 15) most of the variance occurs at synoptic frequencies, whereas at intraseasonal time-scales it produces weak variability with little structure. In contrast, the BM93 scheme has considerably more variance at all time-scales (Fig. 16). At synoptic time-scales the variance occurs predominantly in the Pacific ITCZ and SPCZ, consistent with limited observational data from satellites (e.g. Lau and Chan 1988; Salby *et al.* 1991). Over the Indian Ocean the variance is dominated by intraseasonal time-scales, as was noted by Salby *et al.* (1991). At these lower frequencies two maxima are evident, one over the Indian Ocean and the other over the west Pacific, spreading down into the SPCZ. This pattern is consistent with the spatial

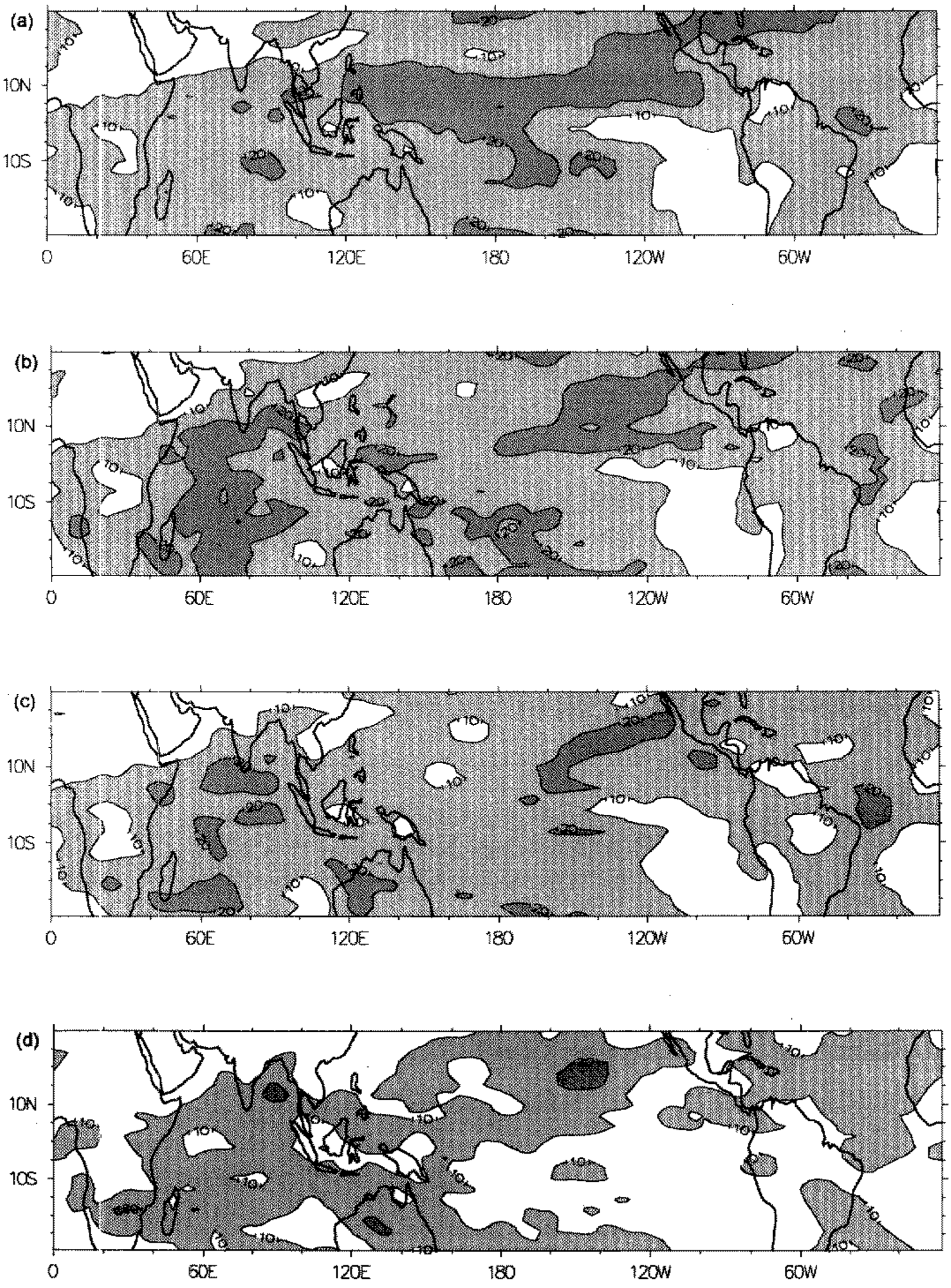

Figure 15. Square root of the variance of the outgoing long-wave radiation (W m^{-2}) for days 60.25 to 360, simulated with the Kuo scheme and explained by frequencies between (a) 2 and 6 days, (b) 6 and 14 days, (c) 14 and 30 days, and (d) 30 and 70 days.

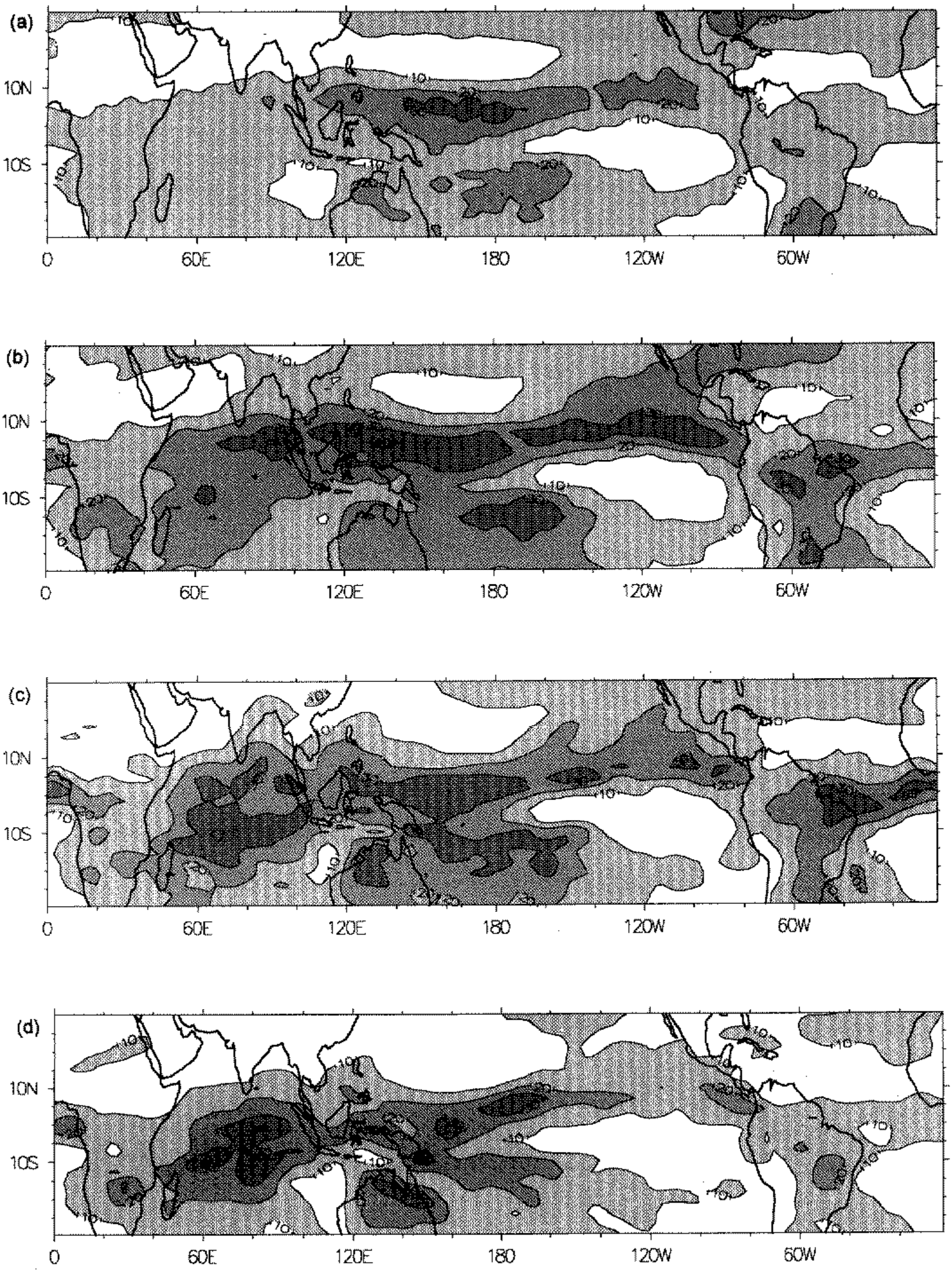

Figure 16. As Fig. 15, but from the Betts and Miller (1993) scheme.

anomalies in the OLR associated with the intraseasonal oscillation (e.g. Knutson and Weickmann 1987; Lau and Chan 1985).

It is clear from the results shown in Figs. 15 and 16 that the model's simulation of tropical variability is highly sensitive to the convective parametrization. Not only are the temporal characteristics and their geographical distribution very different, but also the spatial scale is different. This is demonstrated by the Hofmöller diagrams of the 850 hPa relative vorticity shown in Fig. 17 for the equatorial Pacific, from a typical 90-day period from each integration. With the Kuo scheme (Fig. 17(a)) the synoptic variance seen in Fig. 15(a) is associated with weak lower tropospheric disturbances which propagate westwards around the equatorial belt with a fairly constant phase speed of about 12 m s^{-1}

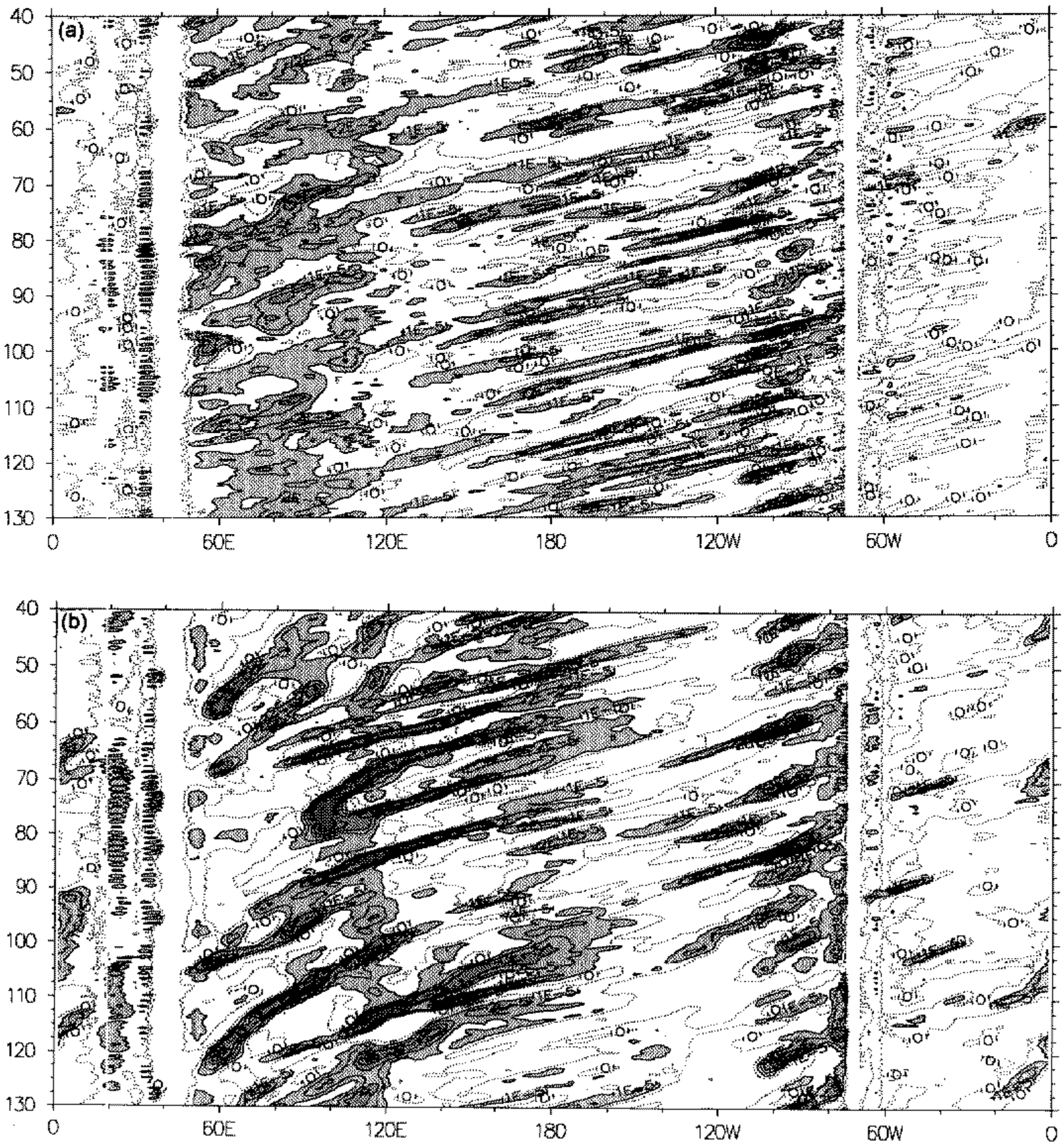

Figure 17. Hofmöller (time/longitude) diagrams of the relative vorticity (s^{-1}) at 850 hPa, along 4°N, from (a) the Kuo scheme, and (b) the Betts and Miller (1993) scheme. The contour interval is 10^{-5} s^{-1}. Only positive (cyclonic) contours are drawn, with the zero contour dotted. Values in excess of 10^{-5} s^{-1} are shaded.

(9° day^{-1}). These quasi-periodic, small-scale features are strongest in the east Pacific, but tend to weaken as they move westwards; over the west Pacific and Indonesia there is little sign of coherent vorticies. Spectra of the relative vorticity show dominant periods of between 3 and 5 days in the central and east Pacific, but no preferred periodicities further west (Fig. 18). Both schemes show the generation of vortices in the east Pacific, to the west of central America. The role of cyclogenesis in the lee of the Sierra Madre mountain range in generating tropical disturbances in the equatorial east Pacific has been proposed by Zehnder and Gall (1991).

With the BM93 scheme the disturbances are larger and more intense (Fig. 17(b)). They appear to be more episodic, with slower and more variable phase speeds. Only over the east Pacific are the waves approximately periodic, with the spectrum displaying a dominant period of 6 days (Fig. 19). Some of these periodic vortices tend to recurve north and eastwards towards the American coast, although some continue to propagate across the equatorial Pacific. There is an indication in Fig. 17(b) that disturbances are generated or intensify near the date-line. This behaviour is consistent with the observed enhancement of convective activity in regions of upper-level westerly flow (e.g. Kiladis and Weickmann 1992). A detailed analysis of the relationship between convection and incursions of extratropical upper tropospheric troughs with this version of the model is in progress.

As the cyclonic vortices propagate westwards they tend to strengthen over the warm pool (Fig. 17(b)), producing disturbances which occupy the depth of the troposphere and give substantial precipitation. Their intensification appears to be intimately related to the development of cold surge events over the South China Sea. Most of the cyclonic disturbances continue westwards into the northern Indian Ocean although a minority migrate polewards into the Pacific storm track. The episodic character of the synoptic waves predicted by the BM93 scheme is similar to the results described by Slingo *et al.* (1992) from a high resolution (T106) version of the ECMWF model which used the mass flux convection scheme of Tiedtke (1989).

A method for objectively tracking a feature and displaying its propagation and development characteristics has been developed recently by Hodges (1994). This technique has been used to study the synoptic variability in the UGCM in more depth. Figure 20 shows examples of the tracks of local maxima in positive (northern hemisphere cyclonic) relative vorticity at 850 hPa based on 6-hourly data for a 90-day period from each integration. The dots on the tracks correspond to the position of the disturbance at each sampling time (i.e. every 6 hours), and the colour of the dot corresponds to the strength of the cyclonic vortex. Thus the technique supplies not only the tracks, but also the propagation speed and the development characteristics of the cyclonic vortices. (Note that the interpolation below orography has produced some spurious features, for example, near the Tibetan plateau.)

Comparison of the tracks produced by each convection scheme (Fig. 20) confirms the conclusions already reached concerning the differing transient characteristics produced by each convection scheme. The rather weak and incoherent nature of the low-level disturbances with the Kuo scheme, particularly over the central and west Pacific, is evident in Fig. 20(a). The strong cyclonic vortices over the east Pacific, the development of new disturbances in the Pacific wave-guide region and their marked intensification over the warm pool, are all clearly seen in Fig. 20(b) for the BM93 scheme. The latitudinal confinement of the ITCZ with the BM93 scheme is also very evident.

Whilst the effect of the tropics on the extratropics is often considered to occur on large space- and time-scales through teleconnection patterns, it may also occur on much shorter scales through the direct poleward migration of tropical disturbances at the

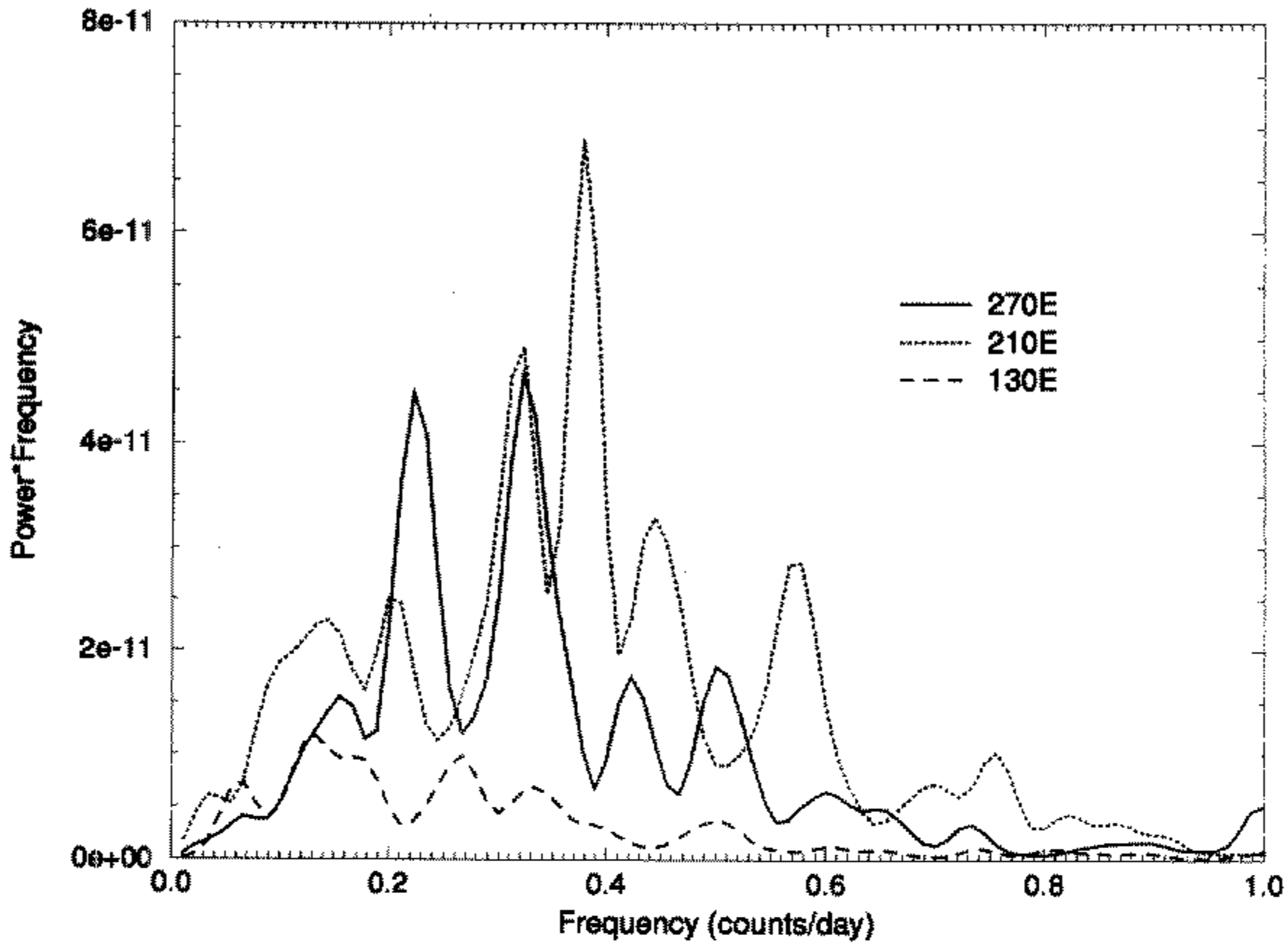

Figure 18. Spectra of the relative vorticity at 850 hPa from three grid points at 4°N over the equatorial Pacific for days 40.25 to 130 from the Kuo scheme. The spectra have been smoothed with a Tukey window.

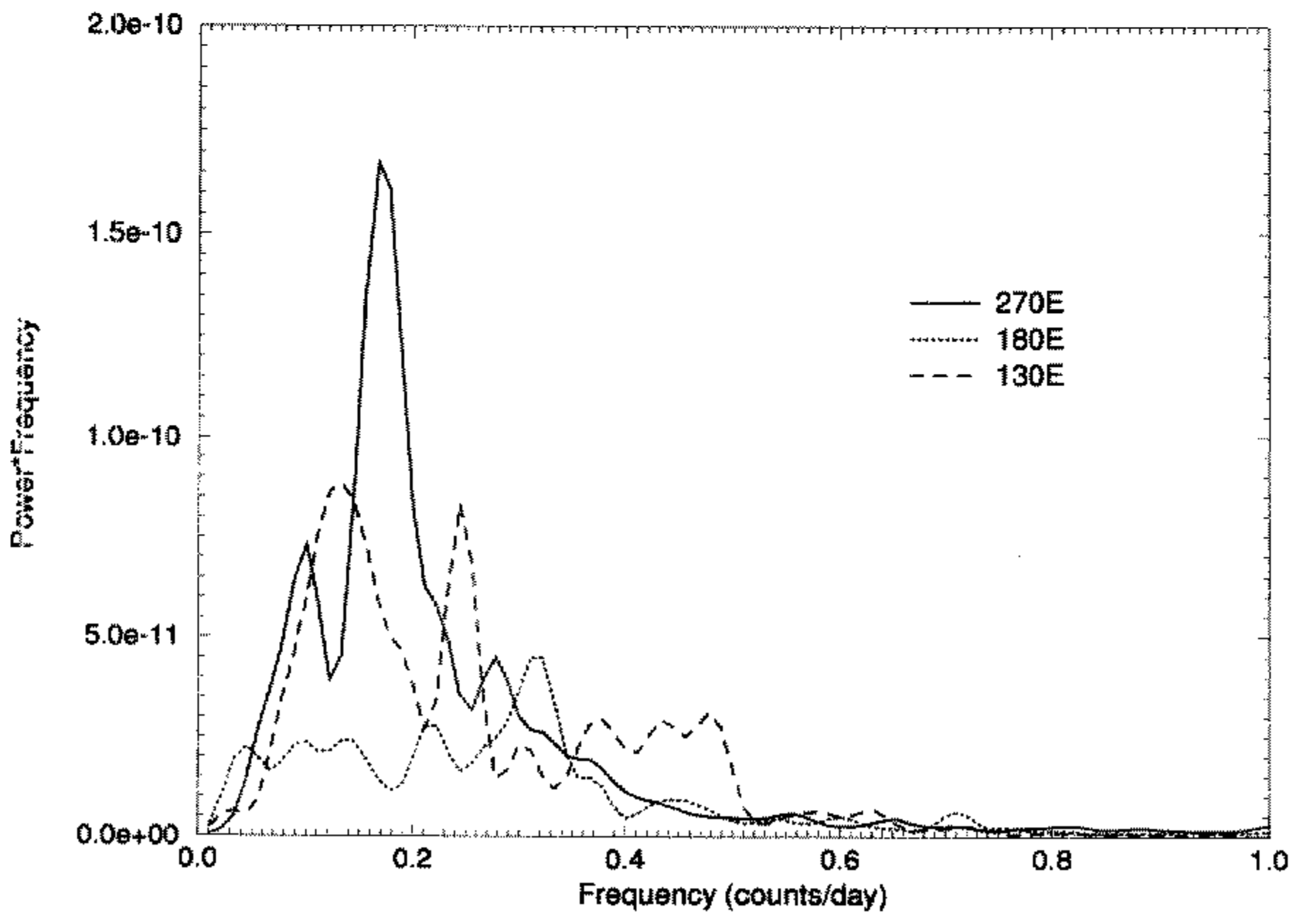

Figure 19. As Fig. 18, but for the Betts and Miller (1993) scheme.

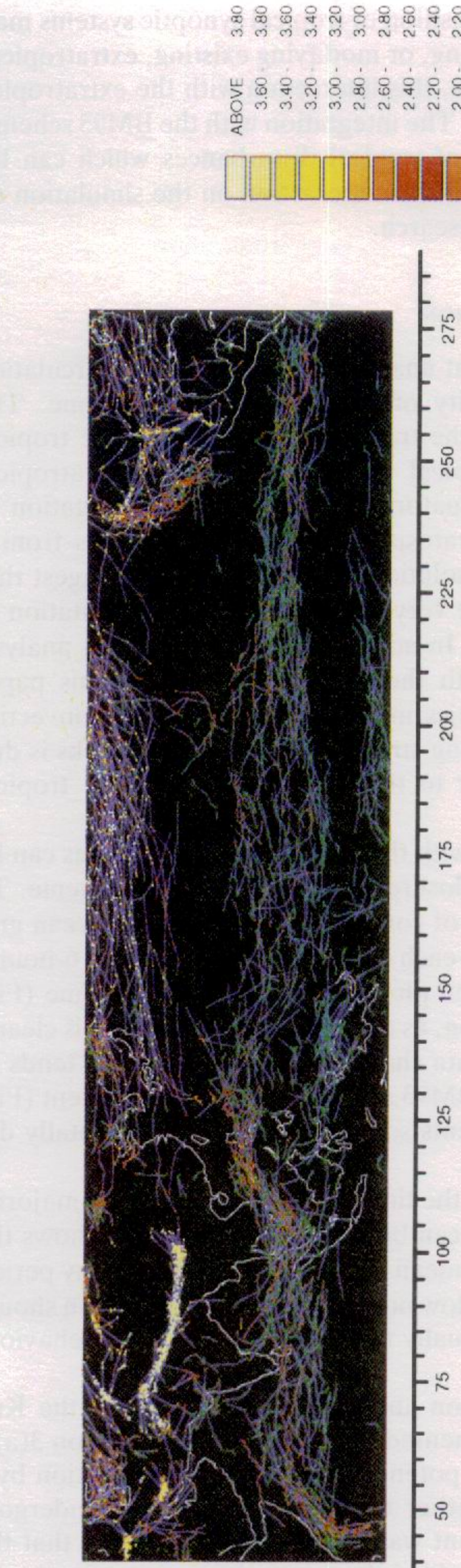

Figure 20. Tracks of 850 hPa relative vorticity maxima (i.e. cylonic in northern hemisphere, anticyclonic in southern hemisphere) from days 270.25 to 360 with (a) the Kuo scheme, and (b) the Betts and Miller (1993) scheme. The colour scale denotes the relative vorticity (10^{-5} s^{-1}).

western boundaries of the major oceans. This transition of tropical synoptic systems may influence the mid-latitude storm tracks by becoming, or modifying existing, extratropical storms (e.g. Walmsley 1993). As Fig. 20 indicates, this interaction with the extratropics is also sensitive to the convective parametrization. The integration with the BM93 scheme shows several examples of poleward migration of tropical disturbances which can be traced to mid-latitude cyclones. The importance of this interaction on the simulation of mid-latitude storm tracks is an area for future research.

7. Discussion

The results described above have shown that analysis of the time-mean circulation is not sufficient to demonstrate the applicability of a parametrization scheme. The substantial differences in the representation of the transient component of the tropical diabatic heating has implications for local tropical weather prediction, extratropical teleconnection patterns, the development of equatorial waves and the propagation of wave energy from the troposphere into the stratosphere. Preliminary results from a version of the UGCM with extended vertical resolution to the mesopause, suggest that the circulation of the middle atmosphere may be very sensitive to the representation of the transient component of tropical convection. In addition, a complementary analysis of the extratropical storm tracks simulated with the integrations used in this paper has demonstrated that the blocking characteristics may be sensitive to the convective parametrization. The degree to which the differing structures of the storm tracks is due to *in situ* changes to the convective heating or to the remote effects of the tropical transience is an area for future research.

The differences in the simulated transience with the Kuo and BM93 schemes can be understood intuitively by considering the basic closure assumptions of each scheme. To aid in this discussion, examples of the evolution of convective rainfall for an ocean grid point over the warm pool are shown in Fig. 21 for each convection scheme. Both 6-hourly mean and daily-mean rainfall amounts have been plotted. With the Kuo scheme (Fig. 21(a)), the pronounced diurnal cycle in convection, as discussed in section 6(b), is clearly evident in the 6-hourly data. The daily-mean data show that the Kuo scheme tends to rain all the time with virtually no dry days. The BM93 scheme is strikingly different (Fig. 21(b)); the rainfall occurs in strong episodic events separated by a series of totally dry days.

The tendency for the Kuo scheme to rain all the time is characteristic of the majority of the tropics with this version of the model, as can be seen in Fig. 22 which shows the percentage frequency of dry days based on daily-mean data from the same 90-day period used in Fig. 21. Even in the subtropics where shallow non-precipitating convection should be occurring, the Kuo scheme still produces virtually no dry days. Again the behaviour of the BM93 scheme is strikingly different.

The persistent widespread weak precipitation and lack of dry days with the Kuo scheme can be explained by its closure as implemented in the UGCM (see section 3(a)). Both schemes initially identify a grid column as potentially undergoing convection by a simple lifting process for near-surface air. Whether that grid column then undergoes precipitating convection is determined in different ways, and it is at this point that the two schemes diverge. With the Kuo scheme, provided there is moisture accession in the previous time step, the scheme will carry out precipitating convection regardless of the humidity profile and the depth of the unstable layer. On the other hand the BM93 scheme first asks whether the profile is sufficiently moist to give precipitation and, second, whether the cloud layer is deep enough (see section 3(b)). If either of these conditions

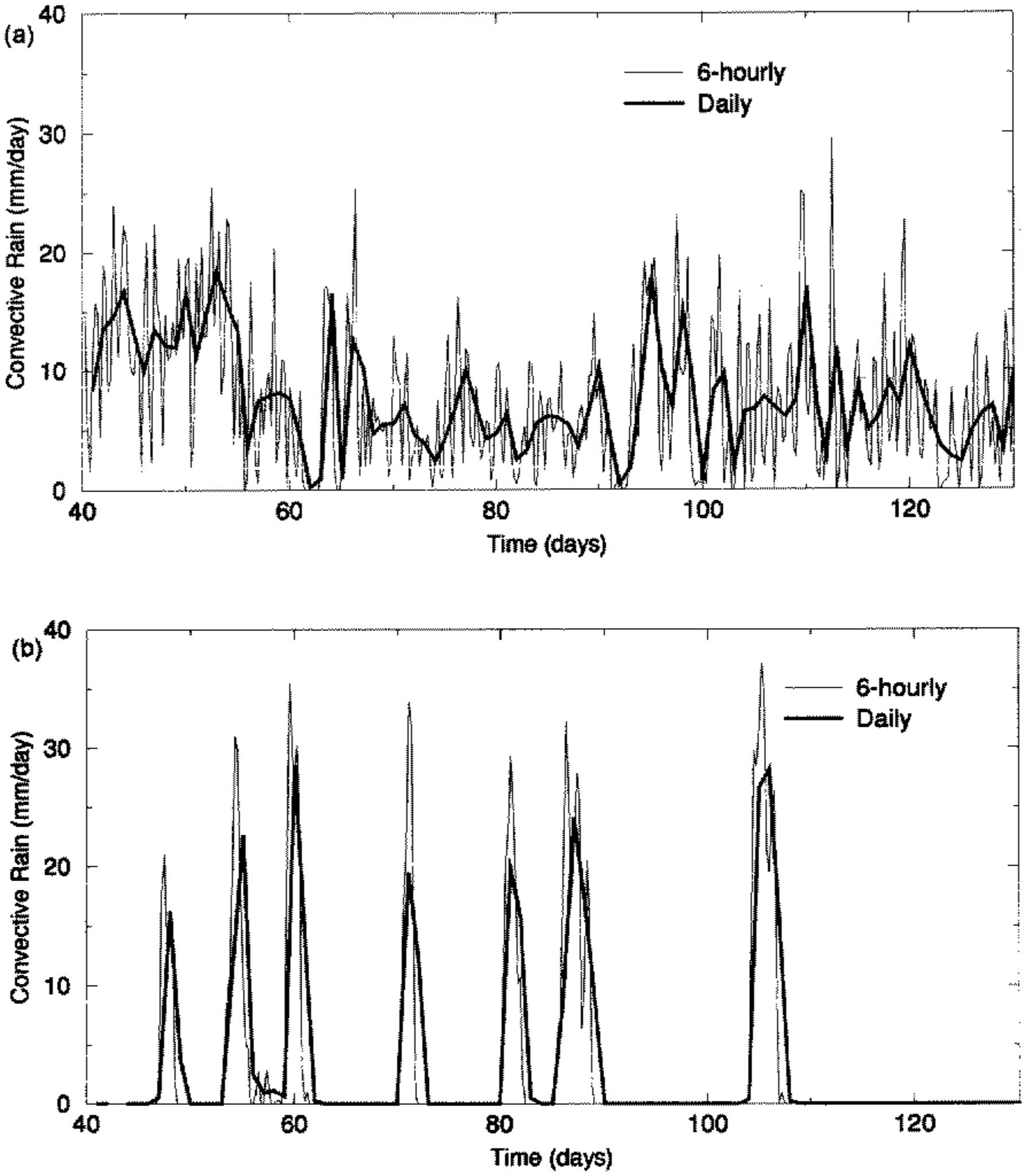

Figure 21. Time series of 6-hourly and daily average convective precipitation at 5°S, 125°E, for days 40.25 to 130 from (a) the Kuo scheme, and (b) the Betts and Miller (1993) scheme.

is not met, then shallow, non-precipitating convection is invoked. Diagnostics obtained during the integration show that, in the majority of cases, it is the moisture condition for the BM93 scheme that decides on the use of shallow rather than deep convection, despite deep instability being diagnosed.

Over a large part of the subtropics, in particular, the atmosphere is not sufficiently moist to support precipitating convection, nor are the clouds of sufficient depth. But since the moisture accession requirement in the Kuo scheme is nearly always met (unless the atmospheric descent is strong enough to counteract the surface evaporation) the scheme will operate over most of the tropical and subtropical oceans. The fact that the scheme only gives dry points over the eastern subtropical oceans is either because the boundary-layer inversion is strong enough to prevent diagnosis of a cloud layer, or because the descent is sufficiently strong for there to be no net moisture accession. Not all versions of the Kuo scheme have such a broad closure for the incidence of convection. In the Bureau of Meteorology Research Centre (BMRC) GCM, the Kuo scheme only operates if the mean relative humidity in the cloud layer exceeds 80% (McAvaney *et al.*

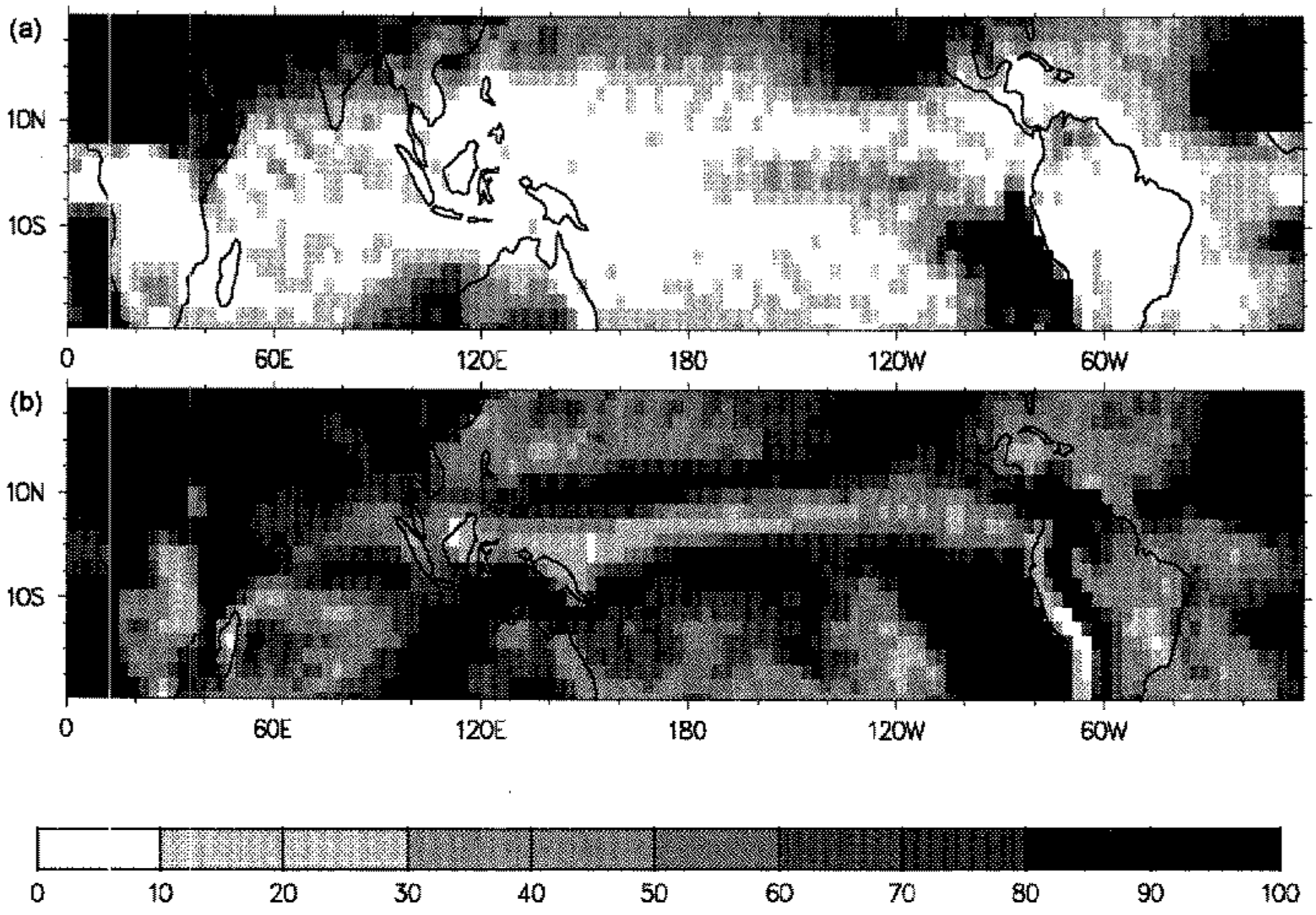

Figure 22. Percentage frequency of dry days (rainfall < 0.01 mm day^{-1}) based on daily average rainfall for days 41 to 130 with (a) the Kuo scheme, and (b) the Betts and Miller (1993) scheme.

1991). Such a constraint would eliminate much of the widespread weak rainfall seen with the version of the Kuo scheme implemented in the UGCM.

With the Kuo scheme, since the moisture accession requirement is nearly always met, and a cloud layer is nearly always diagnosed, the question of whether a grid point precipitates or not then depends on the form of the β-parameter (see Eq. (4), section 3(a)). In the UGCM, the β-parameter is always positive and always less than unity because RH_{crit} has been set to zero. Thus there is always both moistening and heating whatever the moisture profile. The degree of heating depends on the relative humidity of the cloud layer but is alway positive. Since the precipitation is directly related to the heating, the Kuo scheme always produces precipitation regardless of the dryness of the profile.

Thus, both the form of the β-parameter and the logic used for switching between precipitating and non-precipitating convection can explain the areas of widespread weak precipitation in the subtropical anticyclones, regions which should be free of precipitating convection. The introduction of a reasonable critical relative humidity below which only moistening of the profile occurs would certainly be beneficial in eliminating some of this rainfall. Based on observational data, Kuo and Anthes (1984) suggest a value of RH_{crit} between 0.25 and 0.5. This change alone, however, would mean that, in the subtropics, for example, the moistening of the free troposphere would still be achieved by deep, rather than shallow, convective processes, because there is no constraint on the required depth of cloud, as there is in the BM93 scheme. This aspect of the scheme could be improved without difficulty.

The other major shortcoming of the Kuo scheme, as formulated in the UGCM, is its inability to generate the correct modes of tropical transience. The strongest precipitation lies in the central and east Pacific (Fig. 7(a)), associated with the vortices that are shed from central America and which do not intensify further west (Figs. 17(a) and 20(a)). As described in section 3(a) (see Eq. (6)) the scheme is constrained to precipitate only a fraction of the moisture accession in that time step. In a time-mean sense, a balance should exist between moisture accession and precipitation, but this is not necessarily true on an instantaneous basis. Similarly, the coincidence of moisture convergence and convection is a necessary diagnostic relation in the tropics, but it is not clear that it should be a requirement for the initiation of convection at each time step in a GCM, or a limit on the precipitation rate. Instability may be sufficient, such as diurnal heating over land. This constraint may also mean that the Kuo scheme has difficulty in responding to certain perturbations, such as upper tropospheric troughs in the Pacific wave guide. Unlike the Kuo scheme, the BM93 scheme also allows for mid-level convection, which might be important in the initial stages of development of tropical disturbances, and in communicating an upper-level instability through the depth of the tropical troposphere.

The fact that the heating by the Kuo scheme is limited by the moisture accession means that it may have difficulty in initiating a disturbance which would then provide the necessary moisture accession to maintain itself. Also, the heating may then not be sufficiently large to generate the correct transient modes. The warmest regions of the tropics are typically regions where convective heating and ascent (i.e. adiabatic cooling) occur. On average, a balance between the adiabatic and diabatic terms must exist, but on shorter time-scales this may not be so. Idealized models suggest that equatorial modes are excited only when the diabatic heating is large enough to overcome the adiabatic cooling (e.g. Bladé and Hartmann 1993) and hence produce unstable modes. In simple models this is often achieved by using sufficiently warm SSTs, but may also be dependent on the form of the convective parametrization. Thus the constraint on the Kuo scheme that the heating is proportional to the moisture accession may mean that the heating is never sufficiently large to excite strongly the unstable modes. The lack of correlation between warm SSTs and convective activity is indicative of the strength of convection being controlled primarily by the moisture accession rather than by the instability of the atmosphere. In addition, studies with idealized models have suggested that equatorial modes may be sensitive to the vertical structure of the heating profiles (e.g. Lau and Peng 1987). As Fig. 1 indicates, the vertical profile of the convective heating is substantially different with the two schemes. These arguments may need to be studied more conclusively in the context of a simpler, idealized model.

The diverse character of the precipitation processes in each scheme, as indicated by Fig. 21, suggests that the build up and release of convective instability are substantially different. Figure 23 shows the profiles of θ_e from the BM93 scheme, before, during and after the heavy rainfall event near day 105 (Fig. 21(b)). A substantial modification of the profile is evident with the passage of the disturbance. The increase in stability of the air in the middle and lower troposphere occurs over one or two days, and the subsequent destabilization again takes several days to develop. The increase in θ_e in the lower and middle troposphere is primarily due to substantial moistening of the middle and lower troposphere, very similar in magnitude to that reported by Reed and Recker (1971) during the passage of the trough for a composite equatorial Pacific wave. As in Reed and Recker's study the temperature perturbations associated with the disturbance are very small, typically less than 1 K. In contrast, the Kuo scheme shows very little variation in convective instability. Figure 24 shows the extreme limits of the θ_e profiles obtained

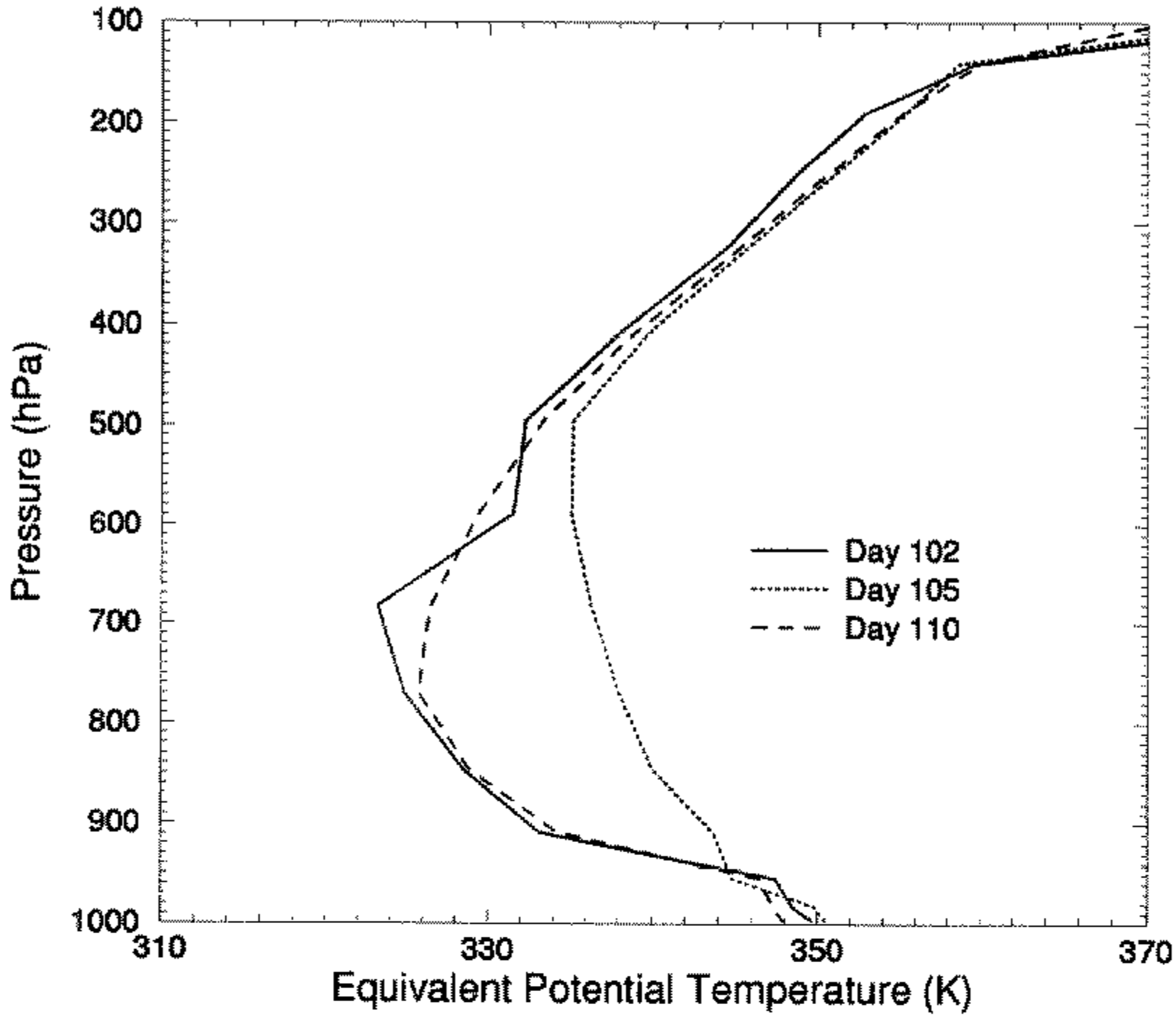

Figure 23. Vertical profiles of equivalent potential temperature at 5°S, 125°E, before, during, and after the passage of a rainfall event with the Betts and Miller (1993) scheme.

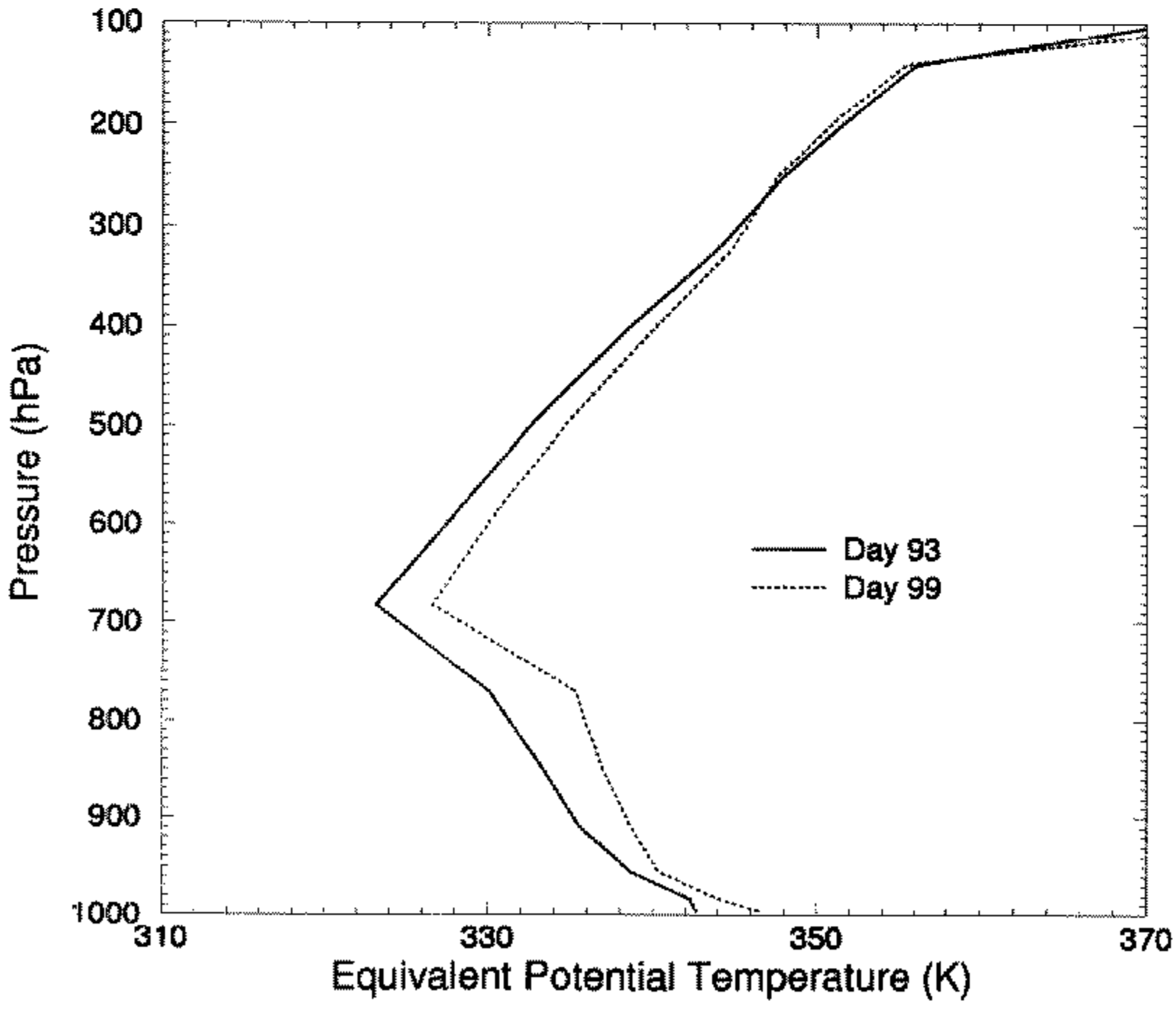

Figure 24. As Fig. 23, but for the extremes of the profiles during a 10-day period with the Kuo scheme

during the 10-day period, days 91 to 100 (see Fig. 21(a)). This result is not surprising, bearing in mind the almost continuous release of precipitation with this form of convective parametrization.

Another feature of the Kuo scheme is its tendency to form a split ITCZ, particularly in the west Pacific (Fig. 8(a)). This characteristic has been noted in other convective parametrizations which use moisture convergence closure (e.g. Tiedtke 1989, and see Miller *et al.* (1992)) and has led to the hypothesis that this closure may be responsible (Hess *et al.* 1993). Certainly, frictional convergence cannot be maintained on the equator because of the Coriolis parameter. Thus, in the case of a uniform surface evaporation field, for example, such schemes would preferentially form disturbances off the equator. In both the ECMWF model (Miller *et al.* 1992) and the UGCM with the Kuo scheme, the partial elimination of the split ITCZ has been achieved by enhancement of surface fluxes at low wind speeds, but the tendency for such a structure still remains. A recent experiment with the BM93 scheme in which the enhancement of the surface fluxes (as described in section 2(b)) was removed has shown that this convection scheme is not at all sensitive to this change. It is able to simulate the necessary intensity and geographical distribution of diabatic heating required to maintain a reasonable tropical circulation without this additional moisture supply.

It is not known how much the substantial differences in the transient characteristics of the Kuo and BM93 schemes described in this paper are features of other convective parametrization schemes. At horizontal resolutions lower than that used in this paper, and typical of many previous climate simulations, the sensitivity to convective parametrization may be quite different since the resolved synoptic scales will vary. It is clear from the above discussion that a study of the temporal characteristics of a convection scheme is essential if the correctness of the closure assumptions are to be assessed. The normal practice of initially tuning a convection scheme by testing it on observed data such as the GARP* Atlantic Tropical Experiment (GATE) wave composites (e.g. Tiedtke 1989) may not be a sufficient test of a scheme, since the disturbance, and hence the moisture accession, is already in place. There appears to be no systematic way of testing the schemes to ensure that they are capable of generating the correct modes of tropical transience. The use of idealized models may be appropriate as a guide to the correctness of any closure assumptions. For the full GCM it is essential to obtain more validation data that describe the temporal characteristics of convection, their seasonal and interannual variability. Satellite observations, such as the initial analysis of ISCCP data presented by Salby *et al.* (1991), may be particularly relevant. Similarly, suitable studies of NWP analyses, such as those described by Lau and Lau (1990), may be useful.

8. Conclusions

In this paper a basic description of the transient characteristics of tropical convection has been presented. It is clear that the BM93 scheme has some skill in simulating the various scales of tropical variability. This variability is built up from the effects of various specific phenomena which, in January, can be identified as cold surges in the west Pacific, interaction with extratropical upper tropospheric troughs in the Pacific wave guide, and intraseasonal oscillations over the eastern hemisphere. The simulation of these phenomena and the interaction between them, as simulated with the BM93 scheme, are to be described in detail in a later paper.

* Global Atmospheric Research Program—a joint project of the World Meteorological Organization and the International Council of Scientific Unions.

Although the results described in this paper suggest that the Kuo scheme may not represent an appropriate parametrization of convective processes, there are clearly a large number of ways to implement such a scheme. Several aspects of the closure used in the UGCM have been identified as problematic and a fuller study of these parameters is planned with an idealized model and the full GCM.

Acknowledgements

The authors are grateful to Harry Hendon for supplying the figures from the Global Cloud Imagery data. AKB is supported by the National Science Foundation under Grant 90-01960 and by the National Aeronautical and Space Administration under Contract NAS5-31738.

References

Andrews, D. G., Holton, J. R. and Leovy, C. B. 1987 *Middle atmosphere dynamics*. Academic Press

Anthes, R. A. 1977 A cumulus parametrization scheme utilising a one-dimensional cloud model. *Mon. Weather Rev.*, **105,** 270–286

Arpe, K. 1988 'Planetary-scale diabatic forcing errors in the ECMWF model'. Pp. 103–150 in the ECMWF Workshop on diabatic forcing, ECMWF, UK

Asselin, R. 1972 Frequency filter for time integrations. *Mon. Weather Rev.*, **100,** 487–490

Betts, A. K. 1983 Thermodynamics of mixed stratocumulus layers: Saturation point budgets. *J. Atmos. Sci.*, **40**, 2655–2670

1986 A new convective adjustment scheme. I: Observational and theoretical basis. *Q. J. R. Meteorol. Soc.*, **112,** 677–691

Betts, A. K. and Miller, M. J. 1993 The Betts–Miller scheme. Chapter in *The representation of cumulus convection in numerical models of the atmosphere*. Eds. K. A. Emanuel and D. J. Raymond. American Meteorological Society

Bladé, I. and Hartmann, D. L. 1993 Tropical intraseasonal oscillations in a simple nonlinear model. *J. Atmos. Sci.*, **50,** 2922–2939

Boer, G. J., Arpe, K., Blackburn, M., Déqué, M., Gates, W. L., Hart, T. L., Le Treut, H., Roeckner, E., Sheinin, D. A., Simmonds, I., Smith, R. N. B., Tokioka, T., Wetherald, R. T. and Williamson, D. 1991 An intercomparison of the climates simulated by 14 atmospheric general circulation models. WMO/TD No. 425

Ferranti, L., Palmer, T. N., Molteni, F. and Klinker, E. 1990 Tropical–extratropical interaction associated with the 30–60 day oscillation and its impact on medium and extended range prediction. *J. Atmos. Sci.*, **47,** 2177–2199

Gates, W. L. 1992 AMIP: The Atmospheric Model Intercomparison Project. *Bull. Am. Meteorol. Soc.*, **73,** 1962–1970

Gent, P. R. 1991 The heat budget of the TOGA-COARE domain in an ocean model. *J. Geophys. Res.*, **96,** 3323–3330

Hartmann, D. L. and Recker, E. E. 1986 Diurnal variation of outgoing longwave radiation in the tropics. *J. Clim. Appl. Meteorol.*, **25,** 800–812

Hendon, H. H. and Liebmann, B. 1991 The structure and annual variation of antisymmetric fluctuations of tropical convection and their association with Rossby-gravity waves. *J. Atmos. Sci.*, **48,** 2127–2140

Hess, P. G., Battisti, D. S. and Rasch, P. J. 1993 The maintenance of the intertropical convergence zones and the large-scale tropical circulation on a water-covered earth. *J. Atmos. Sci.*, **50,** 691–713

Hodges, K. 1994 A general method for tracking analysis and its application to meteorological data. *Mon. Weather Rev.*, to appear

Hoskins, B. J., Hsu, H. H., James, I. N., Masutani, M., Sardeshmukh, P. D. and White, G. H. 1989 Diagnostics of the global atmospheric circulation based on ECMWF analyses 1979–1989. WCRP-27, World Meteorological Organization, Geneva

Hsu, H-H. and Hoskins, B. J. 1989 Tidal fluctuations as seen in ECMWF data. *Q. J. R. Meteorol. Soc.*, **115,** 247–264

Kiladis, G. N. and Weickmann, K. M. 1992 Circulation anomalies associated with tropical convection during northern winter. *Mon. Weather Rev.*, **120,** 1900–1923

Knutson, T. R. and Weickmann, K. M. 1987 30–60 day atmospheric oscillations: Composite life cycles of convection and circulation anomalies. *Mon. Weather Rev.*, **115,** 1407–1436

Kuo, H. L. 1965 On formation and intensification of tropical cyclones through latent heat release by cumulus convection. *J. Atmos. Sci.*, **22,** 40–63

1974 Further studies of the parametrization of the influence of cumulus convection on large-scale flow. *J. Atmos. Sci.*, **31,** 1232–1240

Kuo, Y.-H. and Anthes, R. A. 1984 Semi-prognostic tests of Kuo-type cumulus parametrization schemes in an extratropical convective system. *Mon. Weather Rev.*, **112,** 1498–1509

Lau, K.-H. and Lau, N.-C. 1990 Observed structure and propagation charactertistics of tropical summertime synoptic scale disturbances. *Mon. Weather Rev.*, **118,** 1888–1913

Lau, K.-M. and Chan, P. H. 1985 Aspects of the 40–50 days oscillation during the northern winter as inferred from outgoing longwave radiation. *Mon. Weather Rev.*, **113,** 1889–1909

1988 Interannual and intraseasonal variations of tropical convection: A possible link between the 40–50 day oscillation and ENSO? *J. Atmos. Sci.*, **44,** 506–521

Lau, K.-M. and Peng, L. 1987 Origin of low frequency (intraseasonal) oscillations in the tropical atmosphere. Part I. The basic theory. *J. Atmos. Sci.*, **44,** 950–972

Lau, K.-M., Nakazawa, T. and Sui, C. H. 1991 Observations of cloud cluster hierarchies over the tropical western Pacific. *J. Geophys. Res.*, **96,** 3197–3208

Liebmann, B. and Hendon, H. H. 1990 Synoptic-scale disturbances near the equator. *J. Atmos. Sci.*, **47,** 1463–1479

Madden, R. A. and Julian, P. R. 1972 Description of global-scale circulation cells in the tropics with a 40–50 day period. *J. Atmos. Sci.*, **29,** 1109–1123

McAvaney, B. J., Fraser, J. R., Hart, T. L., Rikus, L. J., Bourke, W. P., Naughton, M. J. and Mullenmeister, P. 1991 'Circulation statistics from a non-diurnal seasonal simulation with the BMRC atmospheric GCM: R21L19'. BMRC Research Report No. 29, Bureau of Meteorology Research Centre, Melbourne, Australia

Miller, M. J. 1988 The sensitivity of systematic errors of the ECMWF forecast model to parametrized processes. Pp. 289–296 in Report No. 12 of CAS/JSC Working Group on numerical experimentation, Workshop on systematic errors in models of the atmosphere, WMO/TD No. 273

Miller, M. J., Beljaars, A. C. M. and Palmer, T. N. 1992 The sensitivity of the ECMWF model to the parametrization of evaporation from tropical oceans. *J. Climate*, **5,** 418–434

Morcrette, J.-J. 1990 Impact of changes to the radiation transfer parametrizations plus cloud optical properties in the ECMWF model. *Mon. Weather Rev.*, **118,** 847–873

Palmer, T. N., Shutts, G. J. and Swinbank, R. 1986 Alleviation of a systematic westerly bias in general circulation and numerical weather prodiction models through an orographic gravity wave drag parametrization. *Q. J. R. Meteorol. Soc.*, **112,** 1001–1039

Palmer, T. N., Branković, C., Molteni, F. and Tibaldi, S. 1990 Extended-range predictions with ECMWF models: Interannual variability in operational model integrations. *Q. J. R. Meteorol. Soc.*, **116,** 799–834

Reed, R. J. and Recker, E. E. 1971 Structure and properties of synoptic-scale wave disturbances in the equatorial western Pacific. *J. Atmos. Sci.*, **28,** 1117–1133

Reed, R. J., Norquist, D. C. and Recker, E. E. 1977 The structure and properties of African wave disturbances as observed during Phase III of GATE. *Mon. Weather Rev.*, **105,** 317–333

Salby, M. L., Hendon, H. H., Woodberry, K. and Tanaka, K. 1991 Analysis of global cloud imagery from multiple satellites. *Bull. Am. Meteorol. Soc.*, **72,** 467–480

Sardeshmukh, P. D. and Hoskins, B. J. 1988 The generation of global rotational flow by steady idealized tropical convergence. *J. Atmos. Sci.*, **45,** 1228–1251

Simmons, A. J. and Burridge, D. M. 1981 An energy and angular momentum conserving vertical finite difference scheme and hybrid vertical coordinate. *Mon. Weather Rev.*, **105,** 758–766

Simmons, A. J., Burridge, D. M., Jarraud, M., Girard, C. and Wergen, W. 1989 The ECMWF medium-range prediction models: Development of the numerical formulations and the impact of increased resolution. *Meteorol. Atmos. Phys.*, **40,** 28–60

Slingo, A. and Slingo, J. M. 1991 Response of the National Center for Atmospheric Research Community Climate Model to improvements in the representation of clouds. *J. Geophys. Res.*, **96,** 15341–15357

Slingo, J. M. 1987 The development and verification of a cloud prediction scheme for the ECMWF model. *Q. J. R. Meteorol. Soc.*, **113,** 899–927

Slingo, J. M., Sperber, K. R., Morcrette, J.-J. and Potter, G. L. 1992 Analysis of the temporal behavior of convection in the tropics of the ECMWF model. *J. Geophys. Res.*, **97,** 18119–18135

Spencer, R. W. 1993 Global oceanic precipitation from the MSU during 1979–91 and comparisons to other climatologies. *J. Climate*, **6,** 1301–1326

Tai, K. S. and Ogura, Y. 1987 An observational study of easterly waves over the eastern Pacific in the northern summer using FGGE data. *J. Atmos. Sci.*, **44,** 339–361

Thuburn, J. 1993 Use of a flux-limited scheme for vertical advection in a GCM. *Q. J. R. Meteorol. Soc.*, **119,** 469–487

Tiedtke, M. 1989 A comprehensive mass-flux scheme for cumulus parametrization in large-scale models. *Mon. Weather Rev.*, **117,** 1779–1800

Tiedtke, M., Heckley, W. A. and Slingo, J. M. 1988 Tropical forecasting at ECMWF: The influence of physical parametrization on the mean structure of forecasts and analyses. *Q. J. R. Meteorol. Soc.*, **114,** 639–664

Walmsley, J. L. 1993 The transatlantic fate of tropical storms. *Weather*, **48,** 350–359

Webster, P. J. 1983 Large-scale structure of the tropical atmosphere. Pp. 235–275 in *Large-scale dynamical processes in the atmosphere.* Eds. B. J. Hoskins and R. P. Pearce. Academic Press

1990 'Ocean–atmosphere interactions in the tropics'. Pp. 67–116 in ECMWF Seminar on tropical extra-tropical interactions. ECMWF, UK

Webster, P. J. and Lukas, R. 1992 TOGA COARE: The Coupled Ocean–Atmosphere Response Experiment. *Bull. Am. Meteorol. Soc.*, **73,** 1377–1416

Yanai, M., Esbensen, S. and Chu, J.-H. 1973 Determination of bulk properties of tropical cloud clusters from large-scale heat and moisture budgets. *J. Atmos. Sci.*, **30,** 611–627

Zehnder, J. A. and Gall, R. L. 1991 On a mechanism for orographic triggering of tropical cyclones in the eastern North Pacific. *Tellus*, **43A,** 25–36